

Construction of Biorthogonal Discrete Wavelet Transforms Using Interpolatory Splines

Amir Z. Averbuch and Valery A. Zheludev

*School of Computer Sciences, Tel Aviv University,
Tel Aviv 69978, Israel*

Communicated by Amos Ron

Received September 21, 1999; revised February 22, 2001

We present a new family of biorthogonal wavelet and wavelet packet transforms for discrete periodic signals and a related library of biorthogonal periodic symmetric waveforms. The construction is based on the superconvergence property of the interpolatory polynomial splines of even degrees. The construction of the transforms is performed in a “lifting” manner that allows more efficient implementation and provides tools for custom design of the filters and wavelets. As is common in lifting schemes, the computations can be carried out “in place” and the inverse transform is performed in a reverse order. The difference with the conventional lifting scheme is that all the transforms are implemented in the frequency domain with the use of the fast Fourier transform. Our algorithm allows a stable construction of filters with many vanishing moments. The computational complexity of the algorithm is comparable with the complexity of the standard wavelet transform. Our scheme is based on interpolation and, as such, it involves only samples of signals and it does not require any use of quadrature formulas. In addition, these filters yield perfect frequency resolution. © 2002 Elsevier Science

1. INTRODUCTION

Since the pioneering paper by Strömberg [18], polynomial splines have had a rich history as a source for wavelet constructions. See, for example, the works of Battle [5] and Lemarié [13], who devised the orthogonal spline wavelet bases, Chui and Wang [6] and Unser, Aldroubi, and Eden [21], who constructed compactly supported semiorthogonal spline wavelets, and one of the authors [25, 26], who developed an efficient technique for constructions and computations using periodic spline wavelets. Cohen, Daubechies, and Feauveau [7] used the splines for the construction of biorthogonal compactly supported wavelets. Aldroubi, Eden, and Unser [1] used the filters that originated from the discretized B-splines for the construction of the multiresolution analysis in the space L_2 . The Hermite splines proved to be useful for building the multiwavelets [9]. Recently, Deslauriers and Dubuc developed interpolatory splines [10, 11], which were applied to wavelet

construction in [12] and [20]. Of course, this list of the applications of the splines to wavelet analysis is far from being complete.

In this work, we employed the classical interpolatory continuous splines in a somewhat nonconventional way, namely, as a tool for devising a fully discrete wavelet scheme.

The interpolatory spline of odd order $2m - 1$ (even degree) with equidistant nodes possesses a remarkable property of superconvergence in the midpoints of the intervals between grid points k/N [24]. In these points, it approximates the smooth function f with an accuracy of $N^{-(2m)}$, whereas the global approximation accuracy is $N^{-(2m-1)}$.

One possible application for the superconvergence property is a fast computation of the approximated discrete Fourier transform (DFT) [24]. Briefly, the idea of the computation is that values of the signal located at odd positions are replaced by values in the midpoints of the spline that interpolates the even values of the signal. Then, the computation of the DFT of the obtained approximated signal is reduced to a computation of the DFT only in the even subarray of the signal, followed by a proper update of the obtained array which aimed to suppress aliasing. It accelerates the implementation by at least 1.6 times compared with the standard fast Fourier transform (FFT) implementation. The algorithm yields a very accurate approximation provided the signal is sufficiently smooth; in other words, it is bandlimited in low frequencies.

If this is not the case, the elimination of the odd subarray could distort the signal significantly. For such signals, it is reasonable to use the values of the interpolatory spline for the prediction rather than the replacement of the odd array. Then, the odd subarray is replaced by the difference between the current and the predicted subarrays. On smooth, well-correlated fragments of the signal, these differences will be near zero, whereas irregular fragments will produce significant differences. This result resembles the operation to the wavelet transform. To further extend this resemblance, we should employ the new odd subarray for updating the existing even subarray. The goal of this update is to smooth the even subarray and thus reduce the aliasing which is a consequence of decimation. The above considerations motivate the development of the proposed framework, which grew into being a biorthogonal wavelet scheme. Based upon the above strategy, we constructed a new family of biorthogonal wavelet and wavelet packet transforms and a related library of biorthogonal symmetric waveforms.

The proposed construction is somewhat related to Donoho's interpolating wavelet construction [12] as it was modified later by Sweldens [20] into what is called the "lifting scheme." In Donoho's scheme for the prediction of the odd subarray, the values of the polynomials, which interpolate the terms of the even array, are used and the odd subarray is replaced by the difference. The even subarray is left unchanged. By introducing the update step, Sweldens [20] modified the construction into being a biorthogonal wavelet transform with compactly supported basic waveforms.

In this paper, we use interpolatory splines instead of polynomials for prediction. As a result, we gain smoother basic waveforms with a refined frequency resolution. On the other hand, these waveforms are not compactly supported and do not have explicit representations in the time domain. Therefore, unlike the conventional lifting scheme, all the computations are conducted in the frequency domain using FFT. A similar scheme can be developed for the implementation of the transforms in the time domain using recursive filters. This is done in [3] for a similar scheme which employed discrete rather than continuous interpolatory splines.

In the following, we outline the main features of the proposed scheme:

- (1) It contains some control tools which allow the construction of a library of biorthogonal filter banks with predetermined properties.
- (2) The decomposition filters that are presented in this paper act as a difference operator of high orders. This property, which we call “quasi-vanishing moments,” is related to vanishing moments properties which characterize wavelet schemes. The proposed approach allows a stable construction of filters with a large number of “quasi-vanishing moments.”
- (3) The filters are linear phase and the basic waveforms are symmetric.
- (4) The proposed wavelet and wavelet packet transforms lead to a refined partition of the frequency domain.
- (5) The computational cost of the transforms is competitive with the cost of the conventional wavelet and wavelet packet transforms.
- (6) The scheme is interpolating, and as such, it operates on samples of signals without the need for quadrature formulas. Moreover, it allows us to stay completely within a discrete setting.

The paper is organized as follows. In Section 2, we introduce the cosine polynomials which are concerned with B -splines which are fundamental for the sequel. The properties of the polynomials are established. We also recall some necessary facts about interpolatory periodic splines. In Section 3, we devise a family of biorthogonal wavelet-type transforms of signals using lifting steps. The lifting scheme that we propose operates in the frequency domain, contrary to the conventional lifting scheme. Both the primal and dual schemes for construction are considered. We emphasize the fact that the lifting scheme together with the proposed construction yields an efficient computational algorithm. Section 4 is devoted to the description of the properties of the constructed filter banks and basic elements of the transforms. As was mentioned above, the filter banks contain some control tools which supply the scheme with means for flexible adaptation. In the end of the section, we show how to use these control tools.

The transforms that are presented in Section 3 are one-level (scale) wavelet-type transforms. They can be decomposed into more scales in two ways. One is the multiscale wavelet transform, where the frequency domain is split in line with the logarithmic scale. Another way is to use the wavelet packet transform, where the partition of the frequency domain is near uniform and it is refined in each subsequent scale of the transform. Both types of transforms, together with the basic waveforms, are described in Section 5. In Section 6, we present a wide collection of filter banks, wavelets, wavelet packets, and their spectra.

2. PERIODIC SPLINES OF EVEN DEGREES

2.1. Preliminaries

Throughout the paper, we assume that $N = 2^j$, $j \in \mathbb{N}$, \sum_k^j stands for $\sum_{k=0}^{2^j-1}$. Denote $\omega_j = e^{2\pi i 2^{-j}}$. The discrete Fourier transform (DFT) of an array $\mathbf{a}^j = \{a_k\}_{k=0}^{2^j-1}$

and its inverse (DFT) are

$$\hat{\mathbf{a}}^j(n) = \sum_k^j \omega_j^{-nk} a_k, \quad a_k = 2^{-j} \sum_n^j \omega_j^{nk} \hat{\mathbf{a}}^j(n).$$

The sequence

$$V_n^j = \frac{\sin(\pi n/N)}{(\pi n/N)}$$

is a set of Fourier coefficients of the 1-periodic central B -spline of the first order on the grid k/N :

$$M_1^j(x) = \begin{cases} 1, & \text{if } x \in [k - 1/2N, k + 1/2N], k \in \mathbb{Z}, \\ 0, & \text{elsewhere.} \end{cases}$$

The central periodic B -spline of order p is the periodic convolution

$$M_p^j(x) = M_{p-1}^j(x) * M_1^j(x) = \sum_{n=-\infty}^{\infty} e^{2\pi i n x} (V_n^j)^p, \quad p \geq 2. \quad (2.1)$$

Note that the B -splines are positive within their support and symmetric around zero. The nodes of B -splines of even orders are located at points $\{k/N\}_{-\infty}^{\infty}$ and the nodes of B -splines of odd orders at points $\{(2k+1)k/2N\}_{-\infty}^{\infty}$.

Define the exponential splines as

$$\begin{aligned} m_p^j(x, r) &\triangleq \frac{1}{N} \sum_k^j \omega_j^{-kr} M_p^j(x + k/N) \\ &= e^{2\pi i r x} \sin^p(\pi r/N) \sum_{l=-\infty}^{\infty} \frac{e^{2\pi i l N x} (-1)^{pl}}{[\pi(r + lN)/N]^p}, \end{aligned} \quad (2.2)$$

where $r = 0, \dots, N-1$. Note that the splines $\{m_p^j(\cdot, r)\}_{r=0}^{2^j-1}$ are orthogonal to each other on the interval $[0, 1]$.

The B -splines can be expressed through the exponential splines:

$$M_p^j(x - k/N) = \sum_r^j \omega_j^{-kr} m_p^j(x, r). \quad (2.3)$$

Equation (2.2) implies the following property of the exponential splines:

$$m_p^j(x - k/N, r) = \omega_j^{-kr} m_p^j(x, r). \quad (2.4)$$

In the sequel, we use two functions that are derived from exponential splines,

$$u_p^j(r) \triangleq m_p^j(0, r) = \frac{1}{N} \sum_k^j \omega_j^{-kr} M_p^j(k/N) = \sin^p(\pi r/N) \sum_{l=-\infty}^{\infty} \frac{(-1)^{lp}}{(\pi(r + lN)/N)^p},$$

$$\begin{aligned} v_p^j(r) &\triangleq \omega^{-r/2} m_p^j\left(\frac{1}{2N}, r\right) = \frac{\omega^{-r/2}}{N} \sum_k^j \omega^{-kr} M_p^j\left(\frac{k}{N} + \frac{1}{2N}\right) \\ &= \sin^p(\pi r/N) \sum_{l=-\infty}^{\infty} \frac{(-1)^{(p+1)l}}{[\pi(r+lN)/N]^p}. \end{aligned}$$

They and their ratio $U_p^j(r) \triangleq v_p^j(r)/u_p^j(r)$ will be of fundamental importance to us.

Due to the symmetry of the B -splines, the functions u_p^j and v_p^j are real-valued cosine polynomials,

$$u_p^j(r) = P_p(\cos(\pi r/N)), \quad v_p^j(r) = Q_p(\cos(\pi r/N)).$$

The cosine polynomials P_p and Q_p were extensively studied in [16, 19]. They are related to the Euler–Frobenius polynomials [15].

Denote $y = \cos(t)$. Let us introduce the continuous functions,

$$u_p(t) \triangleq \sin^p(t) \sum_{l=-\infty}^{\infty} \frac{(-1)^{lp}}{(t + \pi l)^p} \triangleq P_p(y), \quad (2.5)$$

$$v_p(t) \triangleq \sin^p(t) \sum_{l=-\infty}^{\infty} \frac{(-1)^{l(p+1)}}{(t + \pi l)^p} \triangleq Q_p(y), \quad (2.6)$$

$$U_p(t) \triangleq \frac{v_p(t)}{u_p(t)} = \frac{Q_p(y)}{P_p(y)} \triangleq R_p(y). \quad (2.7)$$

The discrete functions u_p^j, v_p^j, U_p^j are sampled versions of the functions,

$$u_p^j(r) = u_p(\pi r/N), \quad v_p^j(r) = v_p(\pi r/N), \quad U_p^j(r) = U_p(\pi r/N). \quad (2.8)$$

In particular, the following important facts [16] were discovered.

PROPOSITION 2.1. *The functions $u_p(t)$ are π -periodic, strictly positive, and symmetric about $t = \pi/2$, where they attain their single minima on the interval $[0, \pi]$. The functions $v_p(t)$ and $U_p(t)$ are 2π -periodic, and $v_p(t + \pi) = -v_p(t)$, $U_p(t + \pi) = -U_p(t)$. Correspondingly, $u_p^j(r)$ are N -periodic and attain their minima at $r = N/2$, $v_p^j(r)$, $U_p^j(r)$ are $2N$ -periodic, and $v_p^j(r + N) = -v_p^j(r)$, $U_p^j(r + N) = -U_p^j(r)$.*

PROPOSITION 2.2. *The following recurrence relations hold,*

$$Q_{p+1}(y) = yQ_p(y) + \frac{1-y^2}{p} \frac{dQ_p(y)}{dy}, \quad Q_2(y) \equiv 1, \quad (2.9)$$

$$P_{p+1}(y) = yP_p(y) + \frac{1-y^2}{p} \frac{dP_p(y)}{dy}, \quad P_1(y) \equiv 1, \quad (2.10)$$

Let us establish some additional properties of the functions u_p , v_p , and U_p^j .

PROPOSITION 2.3. *The following asymptotic relations are true as $t \rightarrow 0$, $p > 2$,*

$$u_p(t) = 1 + O(t^p); \quad v_p(t) = 1 + O(t^p). \quad (2.11)$$

If the parameter p is odd, then

$$u_p(t) - v_p(t) = O(t^{p+1}). \quad (2.12)$$

Proof. The function u_p can be represented as

$$u_p(t) = \sin^p(t)(t^{-p} + A(t)), \quad \text{where } A(t) = \sum_{l=-\infty, l \neq 0}^{\infty} \frac{(-1)^{lp}}{(t + \pi l)^p}.$$

It is readily seen that $A(t) = O(1)$ as $t \rightarrow 0$. Hence, we obtain the first relation of (2.11). The second one is similarly derived.

Assume the parameter p is odd. Then

$$u_p(t) = \sin^p(t) \sum_{l=-\infty}^{\infty} \frac{(-1)^l}{(t + \pi l)^p}, \quad v_p(t) = \sin^p(t) \sum_{l=-\infty}^{\infty} \frac{1}{(t + \pi l)^p}. \quad (2.13)$$

The difference is

$$u_p(t) - v_p(t) = \sin^p(t)B(t), \quad \text{where } B(t) = \sum_{l=-\infty}^{\infty} (t + \pi(2l + 1))^{-p}.$$

With any $p > 2$, the function B is differentiable and $B(0) = 0$; consequently, $B(t) = O(t)$ as $t \rightarrow 0$. With (2.11) at hand, we derive (2.12). ■

PROPOSITION 2.4. *If the parameter p is odd, then*

$$u_p(\pi - t) = u_p(t), \quad v_p(\pi - t) = -v_p(t), \quad U_p(\pi - t) = -U_p(t).$$

Proof. Follows immediately from (2.13).

COROLLARY 2.1. *If $p > 2$ is odd, then*

$$1 - U_p(t) = \frac{(\cos t - 1)^{(p+1)/2} \xi_p(\cos t)}{u_p(t)},$$

$$1 + U_p(t) = \frac{(-1 - \cos t)^{(p+1)/2} \xi_p(-\cos t)}{u_p(t)},$$

where ξ_p is a polynomial of degree $(p - 3)/2$.

In the following, we present some instances which serve as a basis for further constructions. The functions P_p , Q_p , R_p , that were defined by (2.5)–(2.7), are calculated using the recurrence relations (2.9) and (2.10).

EXAMPLE 2.1.

$$P_3(y) = (1 + y^2)/2, \quad Q_3(y) = y, \quad 1 - R_3(y) = \frac{(1 - y)^2}{1 + y^2},$$

$$1 + R_3(y) = \frac{(1 + y)^2}{1 + y^2}, \quad 1 - R_5(y) = \frac{(y - 1)^3(y - 5)}{5 + 18y^2 + y^4},$$

$$\begin{aligned}
1 - R_7(y) &= \frac{(1-y)^4(y^2 - 28y + 61)}{61 + 479y^2 + 179y^4 + y^6}, \\
1 - R_9(y) &= \frac{(y-1)^5(y^3 - 123y^2 + 1011y - 1385)}{1385 + 19028y^2 + 18270y^4 + 1636y^6 + y^8}, \\
1 - R_{11}(y) &= \frac{(1-y)^6(y^4 - 506y^3 + 11706y^2 - 50666y + 50521)}{50521 + 1073517y^2 + 1949762y^4 + 540242y^6 + 14757y^8 + y^{10}}, \\
1 - R_{13}(y) &= \frac{(1-y)^7(y^5 - 2041y^4 + 11854y^3 - 1212146y^2 + 3448901y - 2702765)}{2702765 + 82112518y^2 + 241595239y^4 + 137963364y^6 + 14494859y^8 + 132854y^{10} + y^{12}}.
\end{aligned}$$

2.2. Interpolatory Splines

The shifts of B -splines form a basis in the space S_p^j of periodic splines of order p on the grid $k/2^j$. Namely, any spline $S_p^j \in S_p^j$ has the following representation:

$$S_p^j(x) = 2^{-j} \sum_k^j q_k^j M_p^j(x - k/N). \quad (2.14)$$

Substituting (2.3) into (2.14), we obtain

$$S_p^j(x) = 2^{-j} \sum_k^j q_k^j \sum_r^j \omega_j^{-kr} m_p^j(x, r) = 2^{-j} \sum_r^j m_p^j(x, r) \sum_k^j q_k^j \omega_j^{-kr}.$$

Denote $\mathbf{q}^j = \{q_k^j\}$. Then

$$S_p^j(x) = 2^{-j} \sum_r^j \xi_r^j m_p^j(x, r), \quad \xi_r^j = \hat{\mathbf{q}}^j(r). \quad (2.15)$$

The values of the spline on the grid points are

$$S_p^j(k/N) = 2^{-j} \sum_r^j \xi_r^j m_p^j(k/N, r).$$

But, due to (2.4),

$$m_p^j(k/N, r) = \omega_j^{kr} m_p^j(0, r) = \omega_j^{kr} u_p^j(r),$$

and we have

$$S_p^j(k/N) = 2^{-j} \sum_r^j \xi_r^j \omega_j^{kr} u_p^j(r),$$

which is the DFT of the N -periodic sequence $\{\xi_r^j u_p^j(r)\}$. Hence, the spline which interpolates the sequence $\mathbf{z}^j = \{z_k\}_{k=0}^{2^j-1}$ is

$$S_p^j(x) = 2^{-j} \sum_r^j \frac{\hat{\mathbf{z}}^j(r)}{u_p^j(r)} m_p^j(x, r).$$

Let us calculate the values of the interpolatory spline in the points $\{(2k + 1)/2N\}$:

$$\begin{aligned}\sigma^j(k) &\triangleq S_p^j(k/N + 1/2N) = 2^{-j} \sum_r^j \xi_r^j m_p^j(k/N + 1/2N, r) \\ &= 2^{-j} \sum_r^j \xi_r^j \omega_j^{kr} m_p^j(1/2N, r) = 2^{-j} \sum_r^j \omega_j^{(k+0.5)r} \hat{\mathbf{z}}^j(r) U_p^j(r).\end{aligned}$$

Hence, we have

$$\hat{\sigma}^j(r) = \omega_j^{r/2} \hat{\mathbf{r}}^j(r) U_p^j(r). \quad (2.16)$$

Our next construction is based on the superconvergence property of the interpolatory splines of odd orders (even degrees).

THEOREM 2.1 [24]. *Let f be a 1-periodic function which has $p + 1$ continuous derivatives and let $S_p^j \in \mathbf{S}_p^j$ interpolate f on the grid $\{k/N\}$. Denote $\tilde{f}_k^j = f(k/N + 1/2N)$. Then in the case of odd $p = 2m - 1$, the following asymptotic relation holds,*

$$\begin{aligned}\sigma^j(k) &= \tilde{f}_k^j + N^{-2m} f^{(2m)} \left(\frac{k}{N} + \frac{1}{2N} \right) (2m - 1)(b_{2m}(0) - b_{2m}(1/2)) \\ &\quad + o(N^{-2m} f^{(2m)}(x)),\end{aligned} \quad (2.17)$$

where $b_s(x)$ is the Bernoulli polynomial of degree s .

Recall that, in general, the interpolatory spline of order $2m - 1$ approximates the function f with accuracy of N^{2m-1} . Therefore, we may claim that $\{k/N + 1/2N\}$ are points of superconvergence of the spline S_p^j or, otherwise, we can say that the spline, which interpolates a smooth function on the grid $\{k/N\}$, quasi-interpolates it in the midpoints $\{k/N + 1/2N\}$.

3. BIORTHOGONAL TRANSFORMS

We switch now to signal processing terminology. The signal f is given on the interval $[0, 1]$ and sampled on the fine grid which is of size $2N$,

$$\mathbf{z}^{j+1} = \{z_k^{j+1} = f(k/2N)\}_{k=0}^{2^{j+1}-1}, \quad N = 2^j.$$

We introduce a family of biorthogonal wavelet-type transforms which we construct through lifting steps. The significant difference with the conventional lifting scheme [20] lies in the fact that here we operate in the frequency domain.

The lifting scheme can be implemented in a primal or a dual mode. We consider both.

3.1. Primal Scheme

3.1.1. Decomposition

Generally, the lifting scheme for decomposition of signals consists of three steps: (1) Split. (2) Predict. (3) Update or lifting. Let us construct and implement our proposed schemes in terms of these steps.

Split. We simply split the array \mathbf{z}^{j+1} into an even $\mathbf{s}^j = \{s_k = z_{2k}^{j+1}\}$ and an odd $\mathbf{d}^j = \{d_k = z_{2k+1}^{j+1}\}_{k=0}^{2^j-1}$ subarray. This is the easiest operation.

Predict. We use the even array \mathbf{s}^j to predict the odd array \mathbf{d}^j and redefine the array \mathbf{d}^j as the difference between the existing array and the predicted one.

To be specific, we use the spline which interpolates the sequence \mathbf{s}^j on the grid k/N ,

$$S_p^j(x) = 2^{-j} \sum_r^j \frac{\hat{\mathbf{s}}^j(r)}{u_p^j(r)} m_p^j(x, r),$$

and predict the array $\hat{\mathbf{d}}^j(r)$ by the array

$$\hat{\sigma}^j(r) = \omega_j^{r/2} \hat{\mathbf{s}}^j(r) U_p^j(r)$$

of the DFT of values of the spline on the points $\{(2k+1)/2N\}$ (see (2.16)). The DFT of the new d -array is defined as follows:

$$\hat{\mathbf{d}}_u^j(r) = \hat{\mathbf{d}}^j(r) - \hat{\sigma}^j(r) = \hat{\mathbf{d}}^j(r) - \omega_j^{r/2} \hat{\mathbf{s}}^j(r) U_p^j(r). \quad (3.1)$$

From now on, the subscript u means update of the array.

Lifting. In this step, we update the even array using the new odd array,

$$\hat{\mathbf{s}}_u^j(r) = \hat{\mathbf{s}}^j(r) + \beta^{j+1}(r) \omega_j^{-r/2} \hat{\mathbf{d}}_u^j(r), \quad (3.2)$$

where $\beta^{j+1}(r)$ is a $2N$ -periodic sequence that is subject to the condition

$$\beta^{j+1}(r+N) = -\beta^{j+1}(r). \quad (3.3)$$

3.1.2. Reconstruction

The reconstruction of the signal \mathbf{z}^{j+1} from the arrays \mathbf{s}_u^j and \mathbf{d}_u^j is implemented in reverse order: (1) Undo lifting. (2) Undo predict. (3) Unsplit.

Undo Lifting. We restore the even array:

$$\hat{\mathbf{s}}^j(r) = \hat{\mathbf{s}}_u^j(r) - \beta^{j+1}(r) \omega_j^{-r/2} \hat{\mathbf{d}}_u^j(r). \quad (3.4)$$

Undo Predict. We restore the odd array:

$$\hat{\mathbf{d}}^j(r) = \hat{\mathbf{d}}_u^j(r) + \omega_j^{r/2} \hat{\mathbf{s}}^j(r) U_p^j(r). \quad (3.5)$$

Let us rewrite (3.5) using (3.4),

$$\begin{aligned}\hat{\mathbf{d}}^j(r) &= \hat{\mathbf{d}}_u^j(r) + \omega_j^{r/2} U_p^j(r) (\hat{\mathbf{s}}_u^j(r) - \beta^{j+1}(r) w_j^{-r/2} \hat{\mathbf{d}}_u^j(r)) \\ &= \hat{\mathbf{d}}_u^j(r) (1 - \beta^{j+1}(r) U_p^j(r)) + \omega_j^{r/2} U_p^j(r) \hat{\mathbf{s}}_u^j(r).\end{aligned}\quad (3.6)$$

Unsplit. The last step represents the standard restoration of the signal from its even and odd components. In the frequency domain, it looks as

$$\hat{\mathbf{z}}^{j+1}(r) = \hat{\mathbf{s}}^j(r) + \omega_j^{-r/2} \hat{\mathbf{d}}^j(r). \quad (3.7)$$

3.2. Dual Scheme

In the primal construction, that was described above, the update step is controlled by the function $\beta^{j+1}(r)$. Now we explain the dual scheme where the prediction step is under control.

3.2.1. Decomposition

(1) We start by updating the even array using the odd array:

$$\hat{\mathbf{s}}_u^j(r) = \frac{1}{2} (\hat{\mathbf{s}}^j(r) + w_j^{-r/2} U_p^j(r) \hat{\mathbf{d}}^j(r)). \quad (3.8)$$

Equation (3.8) means that update is an averaging of the even array with its prediction that was derived from the odd array. Such an update results in a smoother even array.

(2) We form the details array by extracting from the odd array the new even array supplied with the control function $\alpha^{j+1}(r)$:

$$\hat{\mathbf{d}}_u^j(r) = \hat{\mathbf{d}}^j(r) - 2\alpha^{j+1}(r) w_j^{r/2} \hat{\mathbf{s}}_u^j(r).$$

Here $\alpha^{j+1}(r)$ is a $2N$ -periodic sequence and, like $\beta^{j+1}(r)$, $\alpha^{j+1}(r+N) = -\alpha^{j+1}(r)$.

3.2.2. Reconstruction

(1) We restore the odd array

$$\hat{\mathbf{d}}^j(r) = \hat{\mathbf{d}}_u^j(r) + 2\alpha^{j+1}(r) w_j^{r/2} \hat{\mathbf{s}}_u^j(r).$$

(2) To reconstruct the even array, we use $\hat{\mathbf{d}}^j(r)$:

$$\hat{\mathbf{s}}^j(r) = 2\hat{\mathbf{s}}_u^j(r) - w_j^{-r/2} U_p^j(r) \hat{\mathbf{d}}^j(r).$$

(3) Finally,

$$\hat{\mathbf{z}}^{j+1}(r) = \hat{\mathbf{s}}^j(r) + \omega_j^{-r/2} \hat{\mathbf{d}}^j(r).$$

4. FILTER BANKS AND RELATED BASES

4.1. Filter Banks

Lifting schemes, that were presented above, yield an efficient algorithm for the implementation of the forward and backward transform of $\mathbf{z}^{j+1} \longleftrightarrow \{\mathbf{s}_u^j, \mathbf{d}_u^j\}$. But these operations can be interpreted as transformations of the signals by a filter bank that possesses the perfect reconstruction properties.

THEOREM 4.1. (1) *Define the $2N$ -periodic functions*

$$\tilde{g}^{j+1}(r) \triangleq \omega_j^{-r/2}(1 - U_p^j(r)), \quad r = 0, \dots, 2N - 1, \quad (4.1)$$

$$\tilde{h}_\beta^{j+1}(r) \triangleq 1 + \overline{\beta^{j+1}(r)}(1 - U_p^j(r)) = 1 + \overline{\beta^{j+1}(r)}\omega_j^{r/2}\tilde{g}^{j+1}(r), \quad (4.2)$$

$$h^{j+1}(r) \triangleq 1 + U_p^j(r), \quad (4.3)$$

$$g_\beta^{j+1}(r) \triangleq \omega_j^{-r/2}(1 - \beta^{j+1}(r)(1 + U_p^j(r))) = \omega_j^{-r/2}(1 - \beta^{j+1}(r)h^{j+1}(r)). \quad (4.4)$$

Then, the decomposition and reconstruction formulas of the primal scheme can be represented as

$$\hat{\mathbf{s}}_u^j(r) = \frac{1}{2}(\overline{\tilde{h}_\beta^{j+1}(r)}\hat{\mathbf{z}}^{j+1}(r) + \overline{\tilde{h}_\beta^{j+1}(r+N)}\hat{\mathbf{z}}^{j+1}(r+N)), \quad (4.5)$$

$$\hat{\mathbf{d}}_u^j(r) = \frac{1}{2}(\overline{\tilde{g}^{j+1}(r)}\hat{\mathbf{z}}^{j+1}(r) + \overline{\tilde{g}^{j+1}(r+N)}\hat{\mathbf{z}}^{j+1}(r+N)), \quad (4.6)$$

$$\hat{\mathbf{z}}^{j+1}(r) = h^{j+1}(r)\hat{\mathbf{s}}_u^j(r) + g_\beta^{j+1}(r)\hat{\mathbf{d}}_u^j(r). \quad (4.7)$$

(2) *Define the $2N$ -periodic functions*

$$\tilde{H}^{j+1}(r) \triangleq (1 + U_p^j(r))/2, \quad (4.8)$$

$$\tilde{G}_\alpha^{j+1}(r) \triangleq \omega_j^{-r/2}(1 - \alpha^{j+1}(r)(1 + U_p^j(r))) = \omega_j^{-r/2}(1 - 2\alpha^{j+1}(r)\tilde{H}^{j+1}(r)),$$

$$G^{j+1}(r)\omega_j^{-r/2} \triangleq (1 - U_p^j(r)), \quad (4.9)$$

$$H_\alpha^{j+1}(r) \triangleq 2 + 2\alpha^{j+1}(r)(1 - U_p^j(r)) = 2(1 + \alpha^{j+1}(r)\omega_j^{r/2}G^{j+1}(r)). \quad (4.10)$$

Then the decomposition and reconstruction formulas of the dual scheme can be represented as

$$\hat{\mathbf{s}}_u^j(r) = \frac{1}{2}(\overline{\tilde{H}^{j+1}(r)}\hat{\mathbf{z}}^{j+1}(r) + \overline{\tilde{H}^{j+1}(r+N)}\hat{\mathbf{z}}^{j+1}(r+N)),$$

$$\hat{\mathbf{d}}_u^j(r) = \frac{1}{2}(\overline{\tilde{G}_\alpha^{j+1}(r)}\hat{\mathbf{z}}^{j+1}(r) + \overline{\tilde{G}_\alpha^{j+1}(r+N)}\hat{\mathbf{z}}^{j+1}(r+N)),$$

$$\hat{\mathbf{z}}^{j+1}(r) = H_\alpha^{j+1}(r)\hat{\mathbf{s}}_u^j(r) + G^{j+1}(r)\hat{\mathbf{d}}_u^j(r).$$

Proof. We start with the decomposition formula (4.6). Let us modify (3.1) using the identities

$$\begin{aligned} \hat{\mathbf{s}}^j(r) &= (\hat{\mathbf{z}}^{j+1}(r) + \hat{\mathbf{z}}^{j+1}(r+N))/2, \\ \hat{\mathbf{d}}^j(r) &= \omega_j^{r/2}(\hat{\mathbf{z}}^{j+1}(r) - \hat{\mathbf{z}}^{j+1}(r+N))/2. \end{aligned} \quad (4.11)$$

So, we have

$$\begin{aligned}\hat{\mathbf{d}}_u^j(r) &= \frac{\omega_j^{r/2}}{2} (\hat{\mathbf{z}}^{j+1}(r) - \hat{\mathbf{z}}^{j+1}(r+N) - U_p^j(r)(\hat{\mathbf{z}}^{j+1}(r) + \hat{\mathbf{z}}^{j+1}(r+N))) \\ &= \frac{\omega_j^{r/2}}{2} (\hat{\mathbf{z}}^{j+1}(r)(1 - U_p^j(r)) - \hat{\mathbf{z}}^{j+1}(r+N)(1 + U_p^j(r))).\end{aligned}\quad (4.12)$$

But the function $\tilde{g}^{j+1}(r)$, defined in (4.1), possesses the property $\tilde{g}^{j+1}(r+N) = -\omega_j^{-r/2}(1 + U_p^j(r))$. Thus, we see that (4.12) is equivalent to (4.6).

To prove (4.5), we use the identity (4.11) and the already proven relation (4.6). Moreover, we recall that $\omega_j^{-(r+N)/2}\beta^{j+1}(r+N) = \omega_j^{-r/2}\beta^{j+1}(r)$. Then, the decomposition formula (3.2) can be rewritten as

$$\begin{aligned}\hat{\mathbf{s}}_u^j(r) &= \frac{1}{2} (\hat{\mathbf{z}}^{j+1}(r) + \hat{\mathbf{z}}^{j+1}(r+N)) \\ &\quad + \frac{\omega_j^{-r/2}\beta^{j+1}(r)}{2} (\overline{\tilde{g}^{j+1}(r)\hat{\mathbf{z}}^{j+1}(r)} + \overline{\tilde{g}^{j+1}(r+N)\hat{\mathbf{z}}^{j+1}(r+N)}) \\ &= \frac{1}{2} (\hat{\mathbf{z}}^{j+1}(r)(1 + \omega_j^{-r/2}\beta^{j+1}(r)\overline{\tilde{g}^{j+1}(r)}) \\ &\quad + \hat{\mathbf{z}}^{j+1}(r+N)(1 + \omega_j^{-(r+N)/2}\beta^{j+1}(r+N)\overline{\tilde{g}^{j+1}(r+N)})).\end{aligned}$$

Hence (4.5) follows.

To verify the reconstruction formula (4.7), we substitute (3.4) and (3.6) into (3.7).

The relations for the dual scheme are similarly proved. ■

The functions \tilde{h}_β^{j+1} , \tilde{g}^{j+1} , which produced the decomposition of the signal, and h^{j+1} , g_β^{j+1} , which did so for the reconstruction, can be viewed as a perfect reconstruction biorthogonal filter bank. The same is true for the dual functions. Let us verify that they satisfy the perfect reconstruction conditions [17].

THEOREM 4.2. (1) *With any $2N$ -periodic sequence $\beta^{j+1}(r)$ that is subject to the condition $\beta^{j+1}(r+N) = -\beta^{j+1}(r)$, the functions \tilde{h}_β^{j+1} , \tilde{g}^{j+1} , h^{j+1} , g_β^{j+1} satisfy the perfect reconstruction conditions*

$$h^{j+1}(r)\overline{\tilde{h}_\beta^{j+1}(r)} + g_\beta^{j+1}(r)\overline{\tilde{g}^{j+1}(r)} = 2, \quad (4.13)$$

$$h^{j+1}(r)\overline{\tilde{h}_\beta^{j+1}(r+N)} + g_\beta^{j+1}(r)\overline{\tilde{g}^{j+1}(r+N)} = 0, \quad (4.14)$$

(2) *With any $2N$ -periodic sequence $\alpha^{j+1}(r)$ that is subject to the condition $\alpha^{j+1}(r+N) = -\alpha^{j+1}(r)$, the functions \tilde{H}^{j+1} , \tilde{G}_α^{j+1} , H_α^{j+1} , G^{j+1} satisfy the perfect reconstruction conditions*

$$H_\alpha^{j+1}(r)\overline{\tilde{H}^{j+1}(r)} + G^{j+1}(r)\overline{\tilde{G}_\alpha^{j+1}(r)} = 2, \quad (4.15)$$

$$H_\alpha^{j+1}(r)\overline{\tilde{H}^{j+1}(r+N)} + G^{j+1}(r)\overline{\tilde{G}_\alpha^{j+1}(r+N)} = 0. \quad (4.16)$$

Proof. From the definitions (4.1)–(4.4), we derive immediately

$$\begin{aligned}h^{j+1}(r)\overline{\tilde{h}_\beta^{j+1}(r)} + g_\beta^{j+1}(r)\overline{\tilde{g}^{j+1}(r)} &= (1 + U_p^j(r))(1 + \beta^{j+1}(r)(1 - U_p^j(r))) \\ &\quad + (1 - U_p^j(r))(1 - \beta^{j+1}(r)(1 + U_p^j(r))) = 2.\end{aligned}$$

Equations (4.14)–(4.16) can be similarly checked. ■

The following is an obvious observation.

PROPOSITION 4.1. *The filter functions are linked in the following way,*

$$\begin{aligned}\tilde{g}^{j+1}(r) &= \omega_j^{-r/2} h^{j+1}(r+N), & g_\beta^{j+1}(r) &= \overline{\omega_j^{-r/2} \tilde{h}_\beta^{j+1}(r+N)}, \\ G^{j+1}(r) &= 2\omega_j^{-r/2} \tilde{H}^{j+1}(r+N), & \tilde{G}_\alpha^{j+1}(r) &= \omega_j^{-r/2} H_\alpha^{j+1}(r+N)/2.\end{aligned}$$

Moreover, if $\alpha^{j+1}(r) = \beta^{j+1}(r)$, then the decomposition filters of the dual scheme become primal reconstruction filters up to a constant factor and vice versa,

$$\begin{aligned}H_\beta^{j+1}(r) &= 2\tilde{h}_\beta^{j+1}(r), & \tilde{G}_\beta^{j+1}(r) &= g_\beta^{j+1}(r), \\ G^{j+1}(r) &= \tilde{g}^{j+1}(r), & \tilde{H}^{j+1}(r) &= h^{j+1}(r)/2.\end{aligned}\quad (4.17)$$

Remark. Results of this section are related to some extent to the well-known result of Vetterli and Herley [22, Proposition 4.7], which is essential for the construction of the conventional lifting schemes.

4.2. Bases

The perfect reconstruction filter banks, that were constructed above, are associated with the biorthogonal pairs of bases in the space \mathcal{S}^{j+1} of $2N$ -periodic discrete signals.

Notation.

$$\varphi^1(l) \triangleq \frac{1}{2N} \sum_{r=0}^{2N-1} \omega_{j+1}^{rl} h^{j+1}(r), \quad \psi_\beta^1(l) \triangleq \frac{1}{2N} \sum_{r=0}^{2N-1} \omega_{j+1}^{rl} g_\beta^{j+1}(r), \quad (4.18)$$

$$\varphi_\beta^1(l) \triangleq \frac{1}{2N} \sum_{r=0}^{2N-1} \omega_{j+1}^{rl} \tilde{h}_\beta^{j+1}(r), \quad \tilde{\psi}^1(l) \triangleq \frac{1}{2N} \sum_{r=0}^{2N-1} \omega_{j+1}^{rl} \tilde{g}^{j+1}(r). \quad (4.19)$$

DEFINITION 4.1. The functions φ^1 , ψ_β^1 given by (4.18), which belong to the space \mathcal{S}^{j+1} , are called the low-frequency and high-frequency reconstruction wavelets of the first scale, respectively. The functions φ_β^1 , $\tilde{\psi}^1$ given in (4.19), which belong to the space \mathcal{S}^{j+1} , are called the low-frequency and high-frequency decomposition wavelets of the first scale, respectively.

The wavelets in (4.18) and (4.19) are the IDFT of the corresponding filters.

THEOREM 4.3. *The 2-sample shifts of wavelets, defined by (4.18) and (4.19), form biorthogonal pairs of bases in the space \mathcal{S}_{j+1} . This means that any signal $\mathbf{z}^{j+1} \in \mathcal{S}^{j+1}$ can be represented as*

$$z^{j+1}(l) = \sum_{k=0}^{N-1} s_u^j(k) \varphi^1(l-2k) + \sum_{k=0}^{N-1} d_u^j(k) \psi_\beta^1(l-2k), \quad (4.20)$$

and the coordinates are

$$\begin{aligned}s_u^j(k) &= \langle z^{j+1}, \tilde{\varphi}_{\beta,k}^1 \rangle, & \text{where } \tilde{\varphi}_{\beta,k}^1(l) &= \tilde{\varphi}_\beta^1(l-2k), \\ d_u^j(k) &= \langle z^{j+1}, \tilde{\psi}_k^1 \rangle, & \text{where } \tilde{\psi}_k^1(l) &= \tilde{\psi}^1(l-2k).\end{aligned}$$

Proof. We start with the reconstruction formula (4.7), which we rewrite as

$$\hat{\mathbf{z}}^{j+1}(r) = \hat{\mathbf{z}}_h^{j+1}(r) + \hat{\mathbf{z}}_g^{j+1}(r),$$

where

$$\hat{\mathbf{z}}_h^{j+1}(r) \triangleq h^{j+1}(r)\hat{\mathbf{s}}_u^j(r), \quad \hat{\mathbf{z}}_g^{j+1}(r) \triangleq g_\beta^{j+1}(r)\hat{\mathbf{d}}_u^j(r).$$

We have

$$\begin{aligned} z_h^{j+1}(l) &= \frac{1}{2N} \sum_{r=0}^{2N-1} \omega_{j+1}^{rl} h^{j+1}(r) \sum_{k=0}^{N-1} \omega_j^{-rk} s_u^j(k) \\ &= \sum_{k=0}^{N-1} s_u^j(k) \frac{1}{2N} \sum_{r=0}^{2N-1} \omega_{j+1}^{r(l-2k)} h^{j+1}(r) = \sum_{k=0}^{N-1} s_u^j(k) \varphi^1(l-2k). \end{aligned}$$

Similarly, we derive the relation

$$z_g^{j+1}(l) = \sum_{k=0}^{N-1} d_u^j(k) \psi_\beta^1(l-2k).$$

Let us turn to the decomposition formula (4.5). This relation implies that

$$s_u^j(k) = \frac{1}{2N} \sum_{r=0}^{2N-1} \omega_j^{rk} \overline{\tilde{h}_\beta^{j+1}(r)} \hat{\mathbf{z}}^{j+1}(r) = s_u^j(k) = \langle z^{j+1}, \tilde{\varphi}_{\beta,k}^1 \rangle.$$

Similarly, (4.19) is derived. ■

COROLLARY 4.1. *The following biorthogonal relations hold,*

$$\langle \tilde{\varphi}_{\beta,k}^1, \varphi_l^1 \rangle = \langle \psi_{\beta,k}^1, \tilde{\psi}_l^1 \rangle = \delta_k^l, \quad \langle \tilde{\varphi}_{\beta,k}^1, \psi_{\beta,l}^1 \rangle = \langle \tilde{\psi}_l^1, \varphi_k^1 \rangle = 0, \quad \forall l, k.$$

Remark 1. If the function satisfies $\alpha^{j+1}(r) = \beta^{j+1}(r)$, then the decomposition wavelets of the dual scheme are the reconstruction wavelets for the primal one and vice versa.

Remark 2. The basic functions $\varphi^1(l)$ and $\psi_\beta^1(l)$ can be constructed by applying the primal reconstruction procedure to the arrays $s_u^j(k) = \delta_l^k$, $d^j(k) \equiv 0$ and $d_u^j(k) = \delta_l^k$, $s_u^j(k) \equiv 0$, respectively. To construct the decomposition basic functions $\tilde{\varphi}_\beta^1(l)$ and $\psi^1(l)$, we must use the dual reconstruction procedure.

4.3. Control Filters

How do we choose the control filters β for the primal scheme and α for the dual one? Since the decomposition filters in the primal scheme are the reconstruction filters for the dual, we consider $\alpha = \beta$. We emphasize that the perfect reconstruction identities (4.13) and (4.14) for the primal scheme and the corresponding relations for the dual are true for any function β that satisfies the condition (3.3). Thus, by varying the function, we are able to control the decomposition filters $\tilde{h}_\beta^{j+1}(r)$, $\tilde{G}_\beta^{j+1}(r)$ and the reconstruction

filters $H_\beta^{j+1}(r)$, $g_\beta^{j+1}(r)$. We call this group the *beta filters*, whereas the group $\tilde{H}^{j+1}(r)$, $\tilde{g}^{j+1}(r)$, $h^{j+1}(r)$, $G^{j+1}(r)$ is called the *non-beta filters*. We will choose β so that the beta filters have properties which are similar to the properties of the non-beta filters. Since there are several ways to choose the β filters, in the following we present one way to do it according to the above criteria:

(1) Since non-beta filters are functions of $\cos(\pi r/N)$, the wavelets φ^1 and $\tilde{\psi}^1$ are symmetric. If $\beta^{j+1}(r)$ is chosen as a function of $\cos(\pi r/N)$, then the wavelets $\tilde{\varphi}_\beta^1$ and ψ_β^1 are symmetric as well.

(2) Corollary 2.1 implies that the primal decomposition filter $\tilde{g}^{j+1}(r)$ of order p contains the factor

$$D^{p+1} = (1 - \cos(\pi r/N))^{(p+1)/2} = 2^{(p+1)/2} \sin^{p+1}(\pi r/2N).$$

This means that the filter performs as a difference operator of order $p + 1$. This property, which we call “quasi-vanishing moments,” is related to vanishing moments properties which characterize wavelet schemes. Namely, this property can be interpreted as follows: If some fragments of the signal are close to (or coincide with) a polynomial of a degree not exceeding p , then the coefficients $d_u^j(k)$ which are associated with this fragment are near zero. In the frequency domain, the relation $\tilde{g}^{j+1}(r) = O((r/N)^{p+1})$ as $r/N \rightarrow 0$ holds, which guarantees the absence of ripples in the stopband of the filters, especially when p is large. To retain such a valuable property with the dual decomposition filter $\tilde{G}_\beta^{j+1}(r) = w_j^{-r/2}(1 - \beta^{j+1}(r)(1 + U_p^j(r)))$, we necessarily must have $\beta^{j+1}(0) = 1/2$. Let us write $\beta^{j+1}(r) = 1/2 + \theta^{j+1}(r)$, $\theta^{j+1}(0) = 0$. Then

$$\tilde{G}_\beta^{j+1}(r) = w_j^{-r/2}((1 - U_p^j(r))/2 + \theta^{j+1}(r)(1 + U_p^j(r))) = O((r/N)^{p+1}) + \theta^{j+1}(r)O(1).$$

Thus, we can see that the decay of the filter as $r/N \rightarrow 0$ is determined by the behavior of θ in the vicinity of zero, and its order does not exceed $O((r/N)^{p+1})$. If $\theta^{j+1}(r)$ contains the factor D^l , $l \leq p + 1$, then the filter $G_\beta^{j+1}(r)$ operates as a difference operator of order l .

(3) Let us turn to the stopband of the low-pass filter $\tilde{H}^{j+1}(r) = (1 + U_p^j(r))/2$. From Proposition 2.4, we see that $\tilde{H}^{j+1}(r) = (1 - \frac{U_p^j(N-r)}{N})/2 = O(((N-r)/N)^{p+1})$ as $(N-r)/N \rightarrow 0$. The filter $\tilde{h}_\beta^{j+1}(r) = 1 + \beta^{j+1}(r)(1 - U_p^j(r))$ will possess a similar property if we require that $\beta^{j+1}(N-r) = -\beta^{j+1}(r)$ (it implies $\beta^{j+1}(N) = -1/2$).

In summary, the required properties for the filter β are

$$\text{The filter } \beta^{j+1}(r) \text{ is a function of } \cos(\pi r/N). \quad (4.21)$$

$$\beta^{j+1}(r) = 1/2 + \theta^{j+1}(r), \quad \theta^{j+1}(r) \text{ comprises the factor } D^l, \quad l \leq p + 1. \quad (4.22)$$

$$\beta^{j+1}(N-r) = -\beta^{j+1}(r). \quad (4.23)$$

We may argue that an ideal β candidate, which meets the requirements for the order $p = 2m + 1$, is $\beta^{j+1}(r) = U_{2l+1}^j(r)/2$, $l = 1, \dots, m$.

Another suggestion for the choice of β is yielded by the following consideration. Generally, the high- and low-frequency wavelets $\varphi^1(l)$ and $\psi_\beta^1(l)$, respectively, are not orthogonal to each other; this holds as well for $\tilde{\varphi}_\beta^1$ and $\tilde{\psi}^1(l)$. But, by proper choice of the control filter $\beta^{j+1}(r)$, we can achieve this property. In this case, the signals $\mathbf{z}_h^{j+1}(r)$

and $\mathbf{z}_g^{j+1}(r)$, in the representation $\mathbf{z}^{j+1}(r) = \mathbf{z}_h^{j+1}(r) + \mathbf{z}_g^{j+1}(r)$, become orthogonal to each other. Moreover, the decomposition wavelets $\tilde{\varphi}_{\beta,k}^1$ belong to the same subspace as the reconstruction wavelets φ_l^1 . The wavelets $\tilde{\varphi}_{\beta,k}^1$ can be expressed as linear combinations of the wavelets φ_l^1 and vice versa. The same is true for the high-frequency wavelets $\tilde{\psi}_k^1$ and $\psi_{\beta,l}^1$.

PROPOSITION 4.2. *If the control filter $\beta^{j+1}(r)$ is chosen as*

$$\beta^{j+1}(r) = \frac{U_p^j(r)}{1 + (U_p^j(r))^2}, \quad (4.24)$$

then the orthogonal relations

$$\langle \psi_{\beta,k}^1, \varphi_l^1 \rangle = \langle \tilde{\varphi}_{\beta,k}^1, \tilde{\psi}_l^1 \rangle = 0, \quad \forall l, k. \quad (4.25)$$

hold.

Remark. The filter $\beta^{j+1}(r)$, which is given by (4.24), possesses the properties (4.21)–(4.23).

Proof. Using (4.18), we can write

$$\begin{aligned} \langle \psi_{\beta,k}^1, \varphi_l^1 \rangle &= \frac{1}{4N^2} \sum_{n=0}^{2N-1} \sum_{r=0}^{2N-1} \omega_{j+1}^{-r(n-2l)} \overline{h^{j+1}(r)} \sum_{s=0}^{2N-1} \omega_{j+1}^{rl} \omega_{j+1}^{s(n-2k)} g_{\beta}^{j+1}(s) \\ &= \frac{1}{4N^2} \sum_{r,s=0}^{2N-1} \overline{h^{j+1}(r)} g_{\beta}^{j+1}(s) \omega_{j+1}^{2(ks-rl)} \sum_{n=0}^{2N-1} \omega_{j+1}^{-n(s-r)} \\ &= \frac{1}{4N^2} \sum_{r=0}^{2N-1} \overline{h^{j+1}(r)} g_{\beta}^{j+1}(r) \omega_j^{r(k-l)}. \end{aligned}$$

Since $\omega_j^{r(k-l)}$ as a function of r is N -periodic, we represent the inner product as

$$\langle \psi_{\beta,k}^1, \varphi_l^1 \rangle = \sum_{r=0}^{N-1} \omega_j^{r(k-l)} (\overline{h^{j+1}(r)} g_{\beta}^{j+1}(r) + \overline{h^{j+1}(r+N)} g_{\beta}^{j+1}(r+N)).$$

Equations (4.3) and (4.4) imply that

$$\begin{aligned} \overline{h^{j+1}(r)} g_{\beta}^{j+1}(r) &= \omega_j^{-r/2} (1 + U_p^j(r)) (1 - \beta^{j+1}(r) (1 + U_p^j(r))), \\ \overline{h^{j+1}(r+N)} g_{\beta}^{j+1}(r+N) &= -\omega_j^{-r/2} (1 - U_p^j(r)) (1 + \beta^{j+1}(r) (1 - U_p^j(r))). \end{aligned}$$

Hence, we have

$$\langle \psi_{\beta,k}^1, \varphi_l^1 \rangle = \sum_{r=0}^{N-1} \omega_j^{r(k-l-1/2)} (2U_p^j(r) - 2\beta^{j+1}(r) (1 + (U_p^j(r))^2)).$$

Substitution of (4.24) results in $\langle \psi_{\beta,k}^1, \varphi_l^1 \rangle = 0$. The second relation in (4.25) is similarly proved. ■

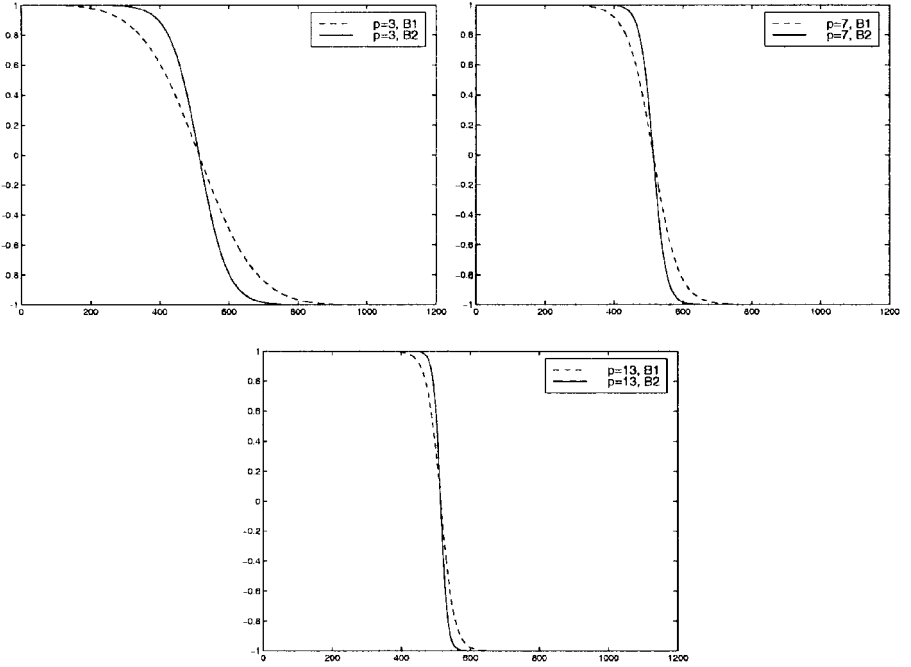


FIG. 1. Functions $\beta^{j+1}(r) = U_p^j(r)/2$ (case B1, dashed lines) and $\beta^{j+1}(r) = U_p^j(r)/(1 + U_p^j(r)^2)$ (case B2, solid lines). In the left picture the case $p = 3$ is displayed; in the central picture, the case $p = 7$ is displayed, and in the right picture, the case $p = 13$ is displayed. $N = 2^{10} = 1024$.

The functions $\beta^{j+1}(r) = U_p^j(r)/2$ and $\beta^{j+1}(r) = U_p^j(r)/(1 + U_p^j(r)^2)$ for $p = 3, 7, 13$ are displayed in Fig. 1. We will depict the filters and wavelets in Section 5.

5. MULTISCALE TRANSFORMS

Repeated applications of the transform can be achieved in an iterative way as was presented above. This can be implemented either as a linear invertible transform of a wavelet type or as a wavelet packet type transform which results in an overcomplete representation of the signal. We explain one multiscale advance as it is done by both transforms.

5.1. The Wavelet Transform

In this transform, we store the array $\hat{\mathbf{d}}_u^j$ and decompose the array \mathbf{s}_u^j . Actually, we employ the DFT arrays $\hat{\mathbf{s}}_u^j(r)$ and $\hat{\mathbf{d}}_u^j(r)$ which were derived in the previous step. The IDFT is applied on the array $\hat{\mathbf{d}}_u^j(r)$ that yields \mathbf{d}_u^j .

Let \mathbf{s}^{j-1} and \mathbf{d}^{j-1} denote the even and odd subarrays of the array \mathbf{s}_u^j . We can find the values of the corresponding DFT directly from $\hat{\mathbf{s}}_u^j(r)$,

$$\begin{aligned}\hat{\mathbf{s}}^{j-1}(r) &= (\hat{\mathbf{s}}_u^j(r) + \hat{\mathbf{s}}_u^j(r + N/2))/2, \\ \hat{\mathbf{d}}^{j-1}(r) &= \omega_p^{r/2} (\hat{\mathbf{s}}_u^j(r) - \hat{\mathbf{s}}_u^j(r + N/2))/2.\end{aligned}$$

In order to produce the new filters, we use a modified version of (2.8) which is

$$u_p^{j-1}(r) = u_p(2\pi r/N), \quad v_p^{j-1}(r) = v_p(2\pi r/N), \quad r = 0, \dots, N/2 - 1.$$

These arrays can be derived by simple downsampling of the arrays $u_p^j(r)$ and $v_p^j(r)$. As for the control filter $\beta^j(r)$, it can be retrieved by downsampling the filter $\beta^{j+1}(r)$, but nothing prevents us from choosing a filter that is completely different from the one used at the first step of the decomposition. We may also choose between the primal and dual schemes for the second-scale transform. The decomposition steps for the primal scheme are:

- (1) $\hat{\mathbf{d}}_u^{j-1}(r) = \hat{\mathbf{d}}^{j-1}(r) - \omega_{j-1}^{r/2} \hat{\mathbf{d}}^{j-1}(r) U_p^{j-1}(r)$.
- (2) $\hat{\mathbf{s}}_u^{j-1}(r) = \hat{\mathbf{s}}^{j-1}(r) + \beta^j(r) \omega_{j-1}^{-r/2} \hat{\mathbf{d}}_u^{j-1}(r)$; $\beta^j(r + N/2) = -\beta^j(r)$.
- (3) The array \mathbf{d}_u^{j-1} is derived by the application of the IDFT. If we terminate the decomposition at this step, we apply the IDFT on $\hat{\mathbf{s}}_u^{j-1}(r)$ as well and produce \mathbf{s}_u^{j-1} . In this event, the original array \mathbf{z}^{j+1} appears as it was transformed into the array $\{\mathbf{d}_u^j, \mathbf{d}_u^{j-1}, \mathbf{s}^{j-1}\}$.

To proceed in getting coarser scales in the decomposition, we use the array $\hat{\mathbf{s}}_u^{j-1}(r)$ rather than \mathbf{s}_u^{j-1} .

The reconstruction steps are:

- (1) Apply the DFT on \mathbf{d}_u^{j-1} . If $\hat{\mathbf{s}}^{j-1}(r)$ is not available from the previous steps of the reconstruction, apply it on \mathbf{s}_u^{j-1} .
- (2) $\hat{\mathbf{s}}^{j-1}(r) = \hat{\mathbf{s}}_u^{j-1}(r) - \beta^j(r) \omega_{j-1}^{-r/2} \hat{\mathbf{d}}_u^{j-1}(r)$.
- (3) $\hat{\mathbf{d}}^{j-1}(r) = \hat{\mathbf{d}}_u^{j-1}(r) + \omega_{j-1}^{r/2} \hat{\mathbf{s}}_u^{j-1}(r) U_p^{j-1}(r)$.
- (4) $\hat{\mathbf{s}}_u^{j-1}(r) = \hat{\mathbf{s}}^{j-1}(r) + \omega_{j-1}^{-r/2} \hat{\mathbf{d}}^{j-1}(r)$.

The dual scheme is implemented in a similar manner. The described transform is linked with the N -periodic filters

$$\begin{aligned} \tilde{h}^j(r) &= \omega_{j-1}^{-r/2} (1 - U_p^{j-1}(r)), & \tilde{h}_\beta^j(r) &= 1 + \overline{\beta^j(r)} \omega_{j-1}^{r/2} \tilde{g}^j(r), \\ h^j(r) &= 1 + U_p^{j-1}(r), & g_\beta^j(r) &:= \omega_{j-1}^{-r/2} (1 - \beta^j(r) h^j(r)). \end{aligned}$$

The filters $\tilde{h}_\beta^j(r)$ and $\tilde{g}^j(r)$ are applied on the array $\hat{\mathbf{s}}_u^j(r)$ to derive $\hat{\mathbf{s}}_u^{j-1}(r)$ and $\hat{\mathbf{d}}_u^{j-1}(r)$. Conversely, $h^j(r)$ and $g_\beta^j(r)$ are applied on the arrays $\hat{\mathbf{s}}_u^{j-1}(r)$ and $\hat{\mathbf{d}}_u^{j-1}(r)$ to restore $\hat{\mathbf{s}}_u^j(r)$.

It is worth noting that the filters $h^j(r)$ and $\tilde{g}^j(r)$ are simple downsampled versions of the filters $h^{j+1}(r)$ and $\tilde{g}^{j+1}(r)$. If the control filter $\beta^j(r)$ is retrieved by downsampling of $\beta^{j+1}(r)$, a similar relation between $h^j(r)$ and $\tilde{h}_\beta^{j+1}(r)$ and $g_\beta^{j+1}(r)$ holds.

The transform can be viewed as an expansion of the signal with a biorthogonal pair of bases:

$$\begin{aligned} z^{j+1}(l) &= \sum_{k=0}^{N/2-1} s_u^{j-1}(k) \varphi^2(l - 4k) + \sum_{k=0}^{N/2-1} d_u^{j-1}(k) \psi_\beta^2(l - 4k) \\ &+ \sum_{k=0}^{N-1} d_u^j(k) \psi_\beta^1(l - 2k). \end{aligned} \quad (5.1)$$

The low-frequency and high-frequency reconstruction wavelets of the second scale are defined as

$$\begin{aligned} \varphi^2(l) &= \frac{1}{2N} \sum_{r=0}^{2N-1} \omega_{j+1}^{rl} h^{j+1}(r) h^j(r), \\ \psi_\beta^2(l) &= \frac{1}{2N} \sum_{r=0}^{2N-1} \omega_{j+1}^{rl} h^{j+1}(r) g_\beta^j(r). \end{aligned} \quad (5.2)$$

The coordinates in (5.1) are inner products with 4-sample shifts of the decomposition wavelets of the second scale,

$$\begin{aligned}\tilde{\varphi}_\beta^2(l) &= \frac{1}{2N} \sum_{r=0}^{2N-1} \omega_{j+1}^{rl} \tilde{h}_\beta^{j+1}(r) \tilde{h}_\beta^j(r), \\ \tilde{\psi}_\beta^2(l) &= \frac{1}{2N} \sum_{r=0}^{2N-1} \omega_{j+1}^{rl} \tilde{h}_\beta^{j+1}(r) \tilde{g}^j(r).\end{aligned}\tag{5.3}$$

The remarks that were made at the end of the previous section remain true for the two-scale transform with obvious modifications.

5.2. The Wavelet Packet Transform

Unlike the mechanism in the wavelet transform, in the wavelet packet transform both subarrays \mathbf{s}_u^j and \mathbf{d}_u^j of the first scale are subject to decomposition that produces four second-scale subarrays. In turn, these four arrays produce eight subarrays for the third scale, and so on. All subarrays which are related to a certain scale are stored.

It is pertinent to re-denote \mathbf{s}_u^j and \mathbf{d}_u^j as $\gamma^{j,0}$ and $\gamma^{j,1}$, respectively. The array $\gamma^{j,0}$ is the source for two second-scale subarrays $\gamma^{j-1,0}$ and $\gamma^{j-1,1}$, whereas $\gamma^{j,1}$ is the source for $\gamma^{j-1,2}$ and $\gamma^{j-1,3}$.

Since $\gamma^{j-1,0}$ and $\gamma^{j-1,1}$ are the arrays \mathbf{s}_u^{j-1} and \mathbf{d}_u^{j-1} , which were discussed in the previous section, we consider only the transform that results in $\gamma^{j-1,2}$ and $\gamma^{j-1,3}$. Unlike the wavelet transform, $\hat{\gamma}^{j,1}(r)$, which is the DFT of the high-frequency array, is being used for multiscale decomposition. As before, we form the arrays

$$\begin{aligned}\hat{\mathbf{S}}^{j-1}(r) &= (\hat{\gamma}^{j,1}(r) + \hat{\gamma}^{j,1}(r + N/2))/2, \\ \hat{\mathbf{D}}^{j-1}(r) &= \omega_{j-1}^{r/2} (\hat{\gamma}^{j,1}(r) - \hat{\gamma}^{j,1}(r + N/2))/2.\end{aligned}$$

Then:

- (1) $\hat{\mathbf{d}}_u^{j-1}(r) = \hat{\mathbf{D}}^{j-1}(r) - \omega_{j-1}^{r/2} \hat{\mathbf{S}}^{j-1}(r) U_p^{-1}(r)$.
- (2) $\hat{\mathbf{s}}_u^{j-1}(r) = \hat{\mathbf{S}}^{j-1}(r) + \tilde{\beta}^j(r) \omega_{j-1}^{-r/2} \hat{\mathbf{d}}_u^{j-1}(r)$; $\tilde{\beta}^j(r + N/2) = -\tilde{\beta}^j(r)$. The control filter $\tilde{\beta}^j(r)$ here can be the same as the filter $\beta^j(r)$, but a different choice is also allowed.
- (3) The arrays of the coefficients are derived by the application of the IDFT,

$$\begin{aligned}\gamma_l^{j-1,2} &= \frac{2}{N} \sum_{r=0}^{N/2-1} \omega_{j-1}^{rl} \hat{\mathbf{d}}_u^{j-1}(r), \\ \gamma_l^{j-1,3} &= \frac{2}{N} \sum_{r=0}^{N/2-1} \omega_{j-1}^{rl} \hat{\mathbf{s}}_u^{j-1}(r).\end{aligned}$$

$\hat{\mathbf{d}}_u^{j-1}(r)$ and $\hat{\mathbf{s}}_u^{j-1}(r)$ are recursively used for further decomposition.

The reconstruction of $\gamma_l^{j,1}$ from $\gamma_l^{j-1,2}$ and $\gamma_l^{j-1,3}$ is implemented in an obvious way.

Similar to the wavelet transform, the wavelet packet transform generates two dual families of basic functions which are called the decomposition and reconstruction wavelet packets. A decomposition of scale j comprises 2^j blocks of basic functions of each family. A block k of scale j consists of 2^j -samples shifts of the decomposition wavelet packet $\tilde{\psi}^{j,k}$

or the reconstruction wavelet packet $\psi^{j,k}$, $k = 0, \dots, 2^j - 1$. The basic functions of any scale form a pair of biorthogonal bases. But there are many more combinations of blocks which do the same [23]. The reconstruction basic function of the block k in scale j can be constructed by launching the primal reconstruction transform from the coefficients of scale j , which are all zeros except for a single coefficient in the block k which is equal to 1. The decomposition basic functions are retrieved similarly by the dual reconstruction transform. We note that, for the first scale, $\psi^{1,0} = \varphi^1$, $\psi_\beta^{1,0} = \varphi_\beta^1$. In the second scale, $\psi^{2,0} = \varphi^2$, $\psi_\beta^{2,1} = \varphi_\beta^2$. Similar relations hold for the decomposition wavelet packets.

6. EXAMPLES

We present here a wide variety of wavelet and wavelet packet filters and basic waveforms that were constructed using the algorithms that were established above.

6.1. Filter Sequences

In this section, we depict the non-beta filter sequences h , \bar{g} of orders $p = 3, 5, 7, 9, 11, 13$ and the beta filter sequences g_β , \bar{h}_β with the same orders. Moreover, we present the beta filters that originated from different choices of the control filter β . This choice is followed from the suggestions proposed in Section 4.3. The filters h , \bar{g} , g_β , \bar{h}_β were defined by (4.1)–(4.4). As it is seen from (4.18) and (4.19), they are the Fourier transforms of the wavelets of the first scale. We depict the wavelets together with the corresponding filters. The indices on the right-hand side of each picture represent the order of the corresponding wavelet.

(1) In Fig. 2, we display the low-frequency φ^1 and the high-frequency ψ_β^1 reconstruction wavelets of the first scale of orders $p = 3, 5, 7, 9, 11, 13$. In addition, their Fourier transforms are also displayed. The Fourier transform of φ^1 is the reconstruction filter sequence h and the Fourier transform of ψ_β^1 is the filter sequence g_β . As it was recommended in Section 4.3, the control filter for the wavelets of order p is chosen as $\beta^{j+1}(r) = U_p^j(r)/2$. Picture A presents the low-frequency wavelets φ^1 from order 3 at the bottom to order 13 at the top. In picture B, their Fourier transforms are shown. These are the filter sequences h . Pictures C and D display the same for the high-frequency wavelets ψ_β^1 and the filters g_β .

(2) Figure 3 depicts in the same way the decomposition wavelets $\tilde{\varphi}_\beta^1$ and $\tilde{\psi}^1$ and the filters \tilde{h}_β and \bar{g} . One can observe that the corresponding decomposition and reconstruction wavelets are similar to each other. The same can be said about the filters. The filters are remarkably flat and have a perfect stopband. The steepness of the cutoff grows together with the order of filter. The spatial localizations of the wavelets, on the contrary, are better when the filter order is low.

(3) In Fig. 4, we display the decomposition low-frequency wavelets $\tilde{\varphi}_\beta^1$ and the reconstruction high-frequency wavelets ψ_β^1 and the corresponding β -filters \tilde{h}_β and g_β for the wavelet of orders $p = 3$ to $p = 13$ with the control filters $\beta^{j+1}(r) = U_p^j(r)/(1 + U_p^j(r)^2)$. By Proposition 4.2, this choice of β guarantees the orthogonality of the wavelets to $\tilde{\psi}^1$ and φ^1 . Comparison with the corresponding wavelets and filters for $\beta^{j+1}(r) =$

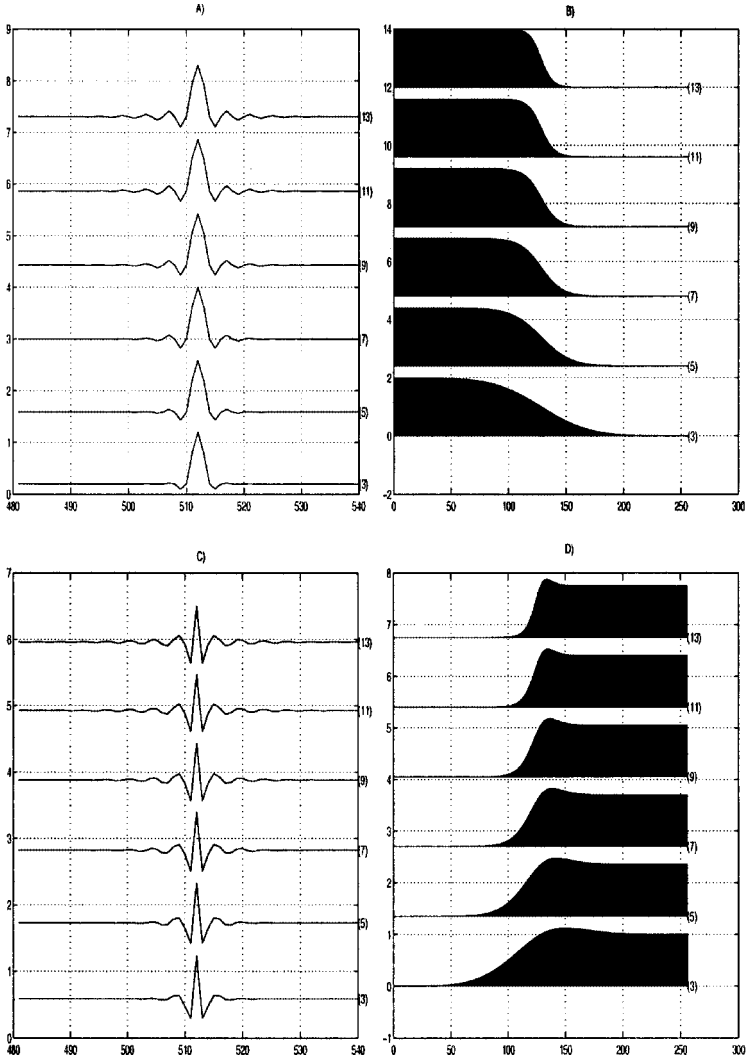


FIG. 2. (A) Low-frequency reconstruction wavelets φ^1 of order $p = 3$ at the bottom to order $p = 13$ at the top. (B) The Fourier transform of A which are the filters h . (C) The high-frequency wavelets ψ_β^1 . (D) The filters g_β for the wavelet of order p . Here the control filter $\beta^{j+1}(r) = U_p^j(r)/2$.

$U_p^j(r)/2$, which are displayed in Figs. 2 and 3, does not reveal a remarkable difference in the appearance between them. The cutoffs of the filters, displayed in Fig. 4 are a little bit steeper than those in Figs. 2 and 3.

(4) The flatness of the filters g_β and \bar{h}_β in Figs. 2, 3, and 4 is disrupted by a bump close to the cutoff point. It could be compensated by the choice $\beta^{j+1}(r) = (U_p^j(r))^p/2$. We illustrate this observation in Fig. 5. The gain in the flatness of the filters was achieved with some sacrifice in spatial localization of the wavelets.

(5) The flatness of the filters can be enhanced together with the improvement of the spatial localization of the wavelets if we are willing to lose some steepness close, to the cutoff point. In Fig. 6, we present the wavelets and the corresponding filters of thirteenth

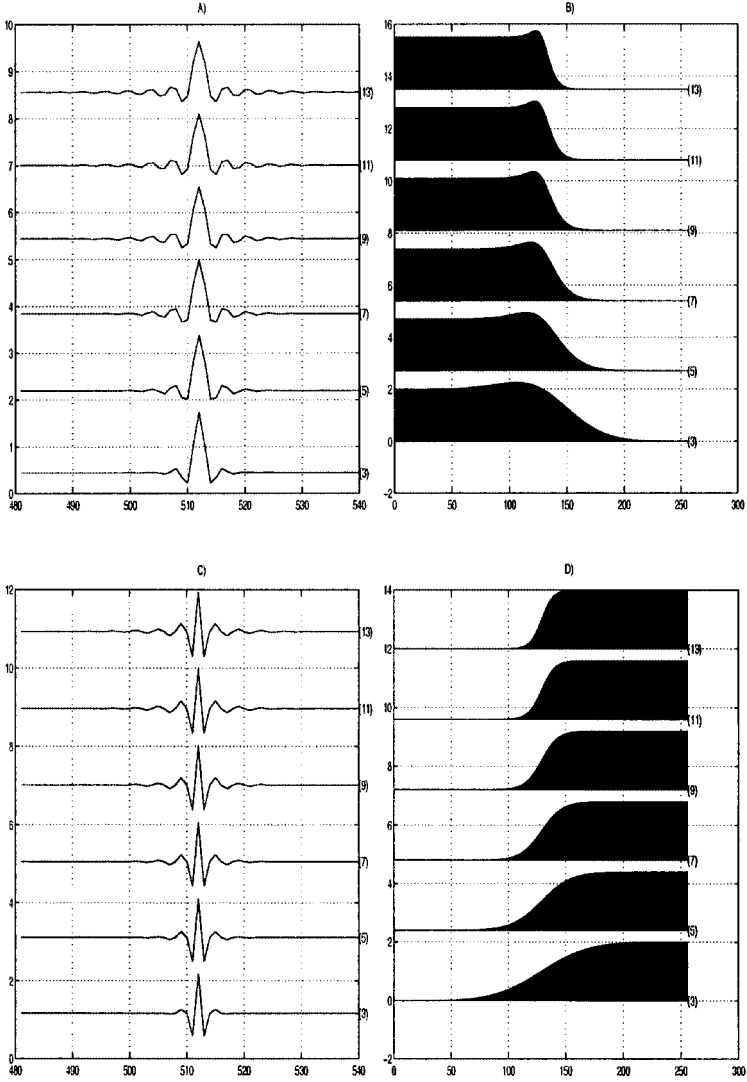


FIG. 3. (A) The decomposition low-frequency wavelets $\tilde{\varphi}_\beta^1$. (B) Their Fourier transforms which are the filters \tilde{h}_β . (C) The high-frequency wavelets $\tilde{\psi}^1$. (D) The filters \tilde{g} for the wavelet of order p . Here $\beta^{j+1}(r) = U_p^j(r)/2$.

order with $\beta^{j+1}(r) = U_l^j(r)/2$, $l = 3, 5, 7, 9, 11, 13$. It exhibits improvements in the flatness of the filters, in the spatial localization of the wavelets, and decay of the cutoff steepness with the decrease of l .

6.2. Wavelets and Wavelet Packets

In this section, we present wavelets in different scales and their spectra. We do so to illustrate the split of the frequency domain by these wavelets. Unlike the nonperiodic case, in a periodic setting the wavelets in different scales cannot be derived by dilations

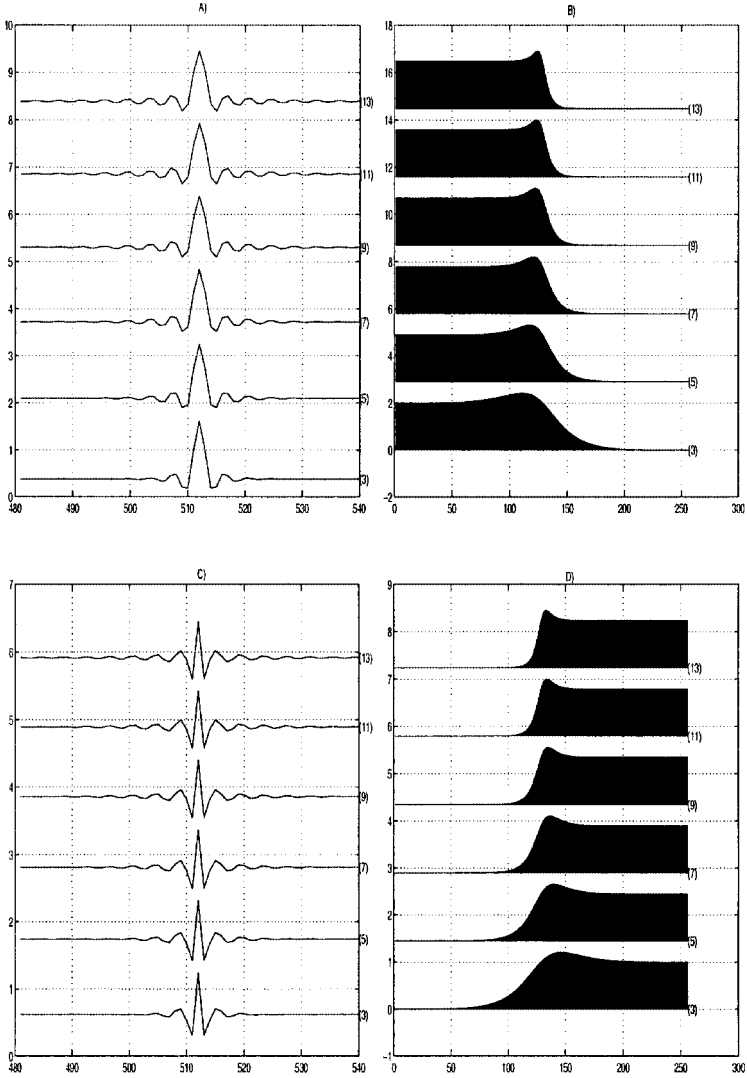


FIG. 4. (A) The decomposition low-frequency wavelets $\tilde{\varphi}_\beta^1$. (B) The filters \tilde{h}_β . (C) The high-frequency wavelets ψ_β^1 . (D) The filters g_β for the wavelet of order p . Here $\beta^{j+1}(r) = U_p^j(r)/(1 + U_p^j(r)^2)$.

of a single wavelet although they are “close” to it. In addition, we also display the wavelet packets and the amplitude of their spectra. The wavelets in the first scale were defined by (5.2) and (5.3). Extension of these definitions to subsequent scales is straightforward. This is also true for wavelet packets. As was noted above, a waveform can be constructed by applying the lifting, reconstruction procedures to the array which contains only one nonzero term. In the following, we display some typical examples of wavelets and wavelet packets of third and thirteenth orders. As for the wavelet packets, we present the packets only in the third scale.

(1) In Fig. 7, we depict the decomposition and reconstruction wavelets of order 3 and their spectra: the high-frequency wavelets $\tilde{\psi}_\beta^l$ and ψ_β^l , $l = 1, \dots, 4$, from the first to the

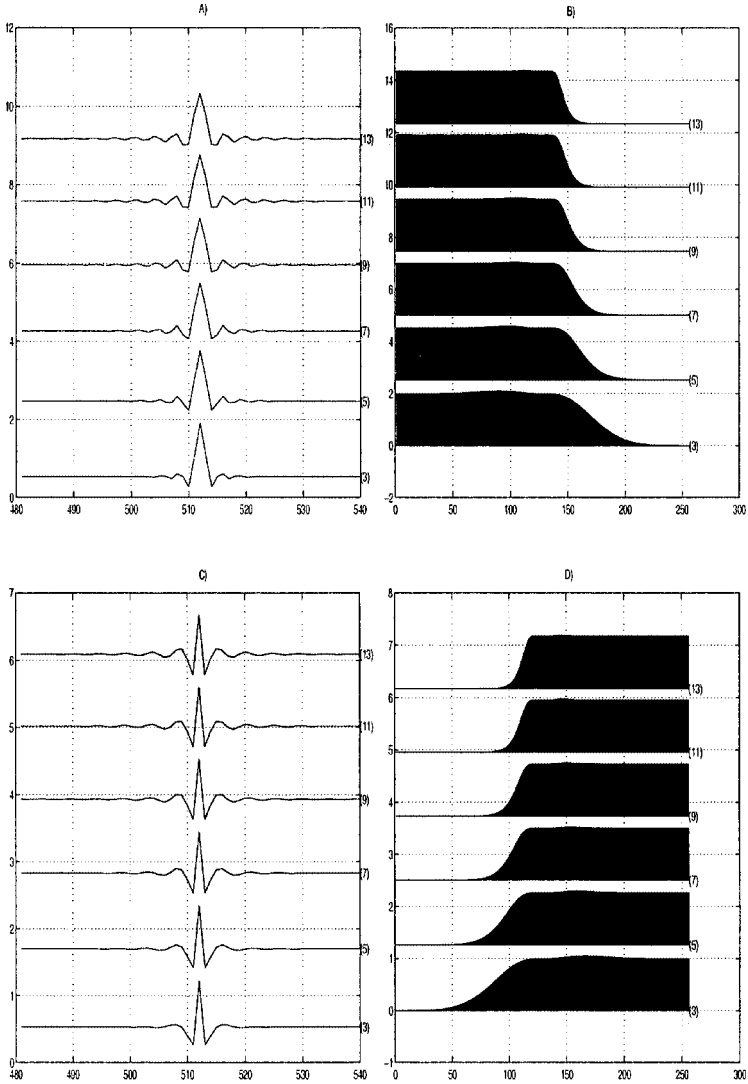


FIG. 5. (A) The decomposition low-frequency wavelets $\tilde{\varphi}_\beta^1$. (B) The filters \tilde{h}_β . (C) The high-frequency wavelets ψ_β^1 . (D) The filters g_β for the wavelet of order p . Here $\beta^{j+1}(r) = (U_p^j(r))^p/2$.

fourth scales and the low-frequency wavelets of the fourth scale $\tilde{\varphi}_\beta^l, \varphi^l, l = 4$. The control filters are chosen to be $\beta^{k+1}(r) = U_3^k(r)/2, k = j + 1 - l$.

(2) In Fig. 8, we do the same for the wavelets of order 13. The control filters are $\beta^{k+1}(r) = U_{13}^k(r)/2, k = j + 1 - l$. By comparing both cases, we can see that the wavelets are well localized in the time domain. The spectra form partitions of the frequency domain according to the logarithmic scale. The corresponding decomposition and reconstruction wavelets are similar in appearance to each other. The third-order wavelets have simpler structure and better localization in time domain than the thirteenth-order wavelets, but the latter form a much more refined partition of the frequency domain.

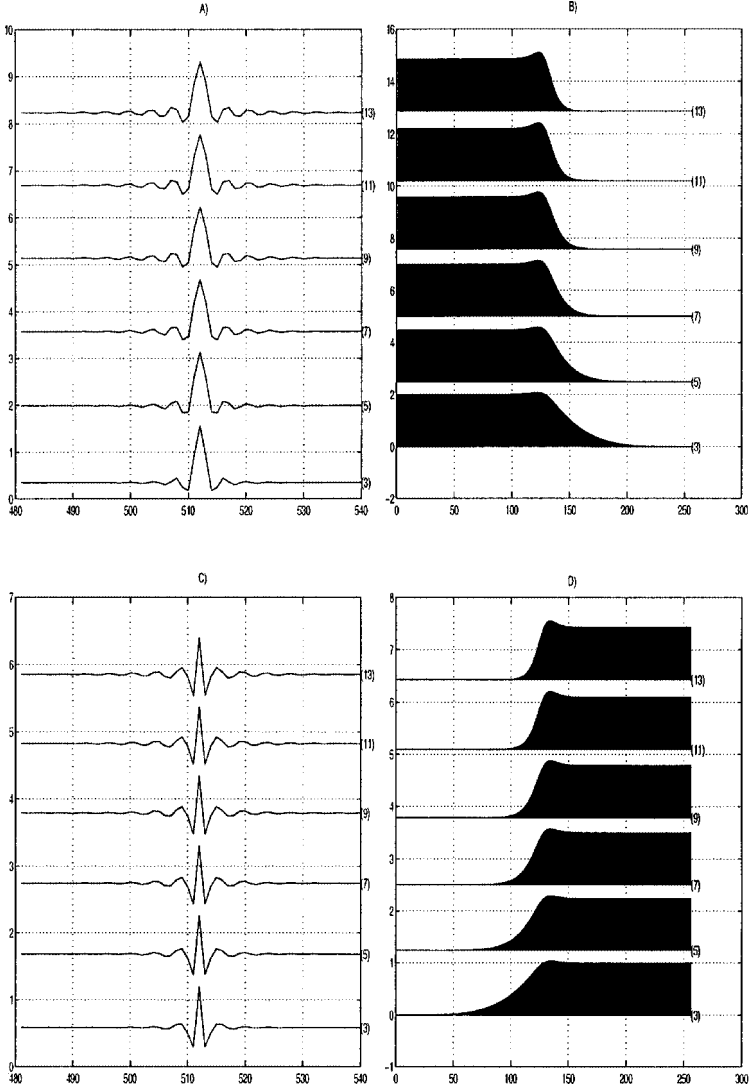


FIG. 6. (A) The decomposition low-frequency wavelets of order 13 $\tilde{\varphi}_\beta^1$. (B) The filters \tilde{h}_β . (C) The high-frequency wavelets ψ_β^1 . (D) The filters g_β . Here $\beta^{j+1}(r) = U_l^j(r)/2, l = 3, 5, 7, 9, 11, 13$.

(3) In Fig. 9, we depict the decomposition and the reconstruction wavelet packets of order 3 for the third scale and their spectra. There are $2^3 = 8$ such wavelet packets for each case.

(4) In Fig. 10, we do the same for the wavelet packets of order 13. The control filters are chosen as $\beta^{k+1}(r) = U_{13}^k(r)/2, k = j + 1 - l$. The wavelet packets form a near-uniform partition of the frequency domain into $2^3 = 8$ blocks. Especially, a refined partition is produced by the reconstruction packets of eleventh order.

(5) We conclude the section with a specific example. Figure 11 depicts the wavelets that were constructed by the alternating scheme. This means that the primal and dual filters alternate from one scale to another. The wavelets of the first scale displayed in A are

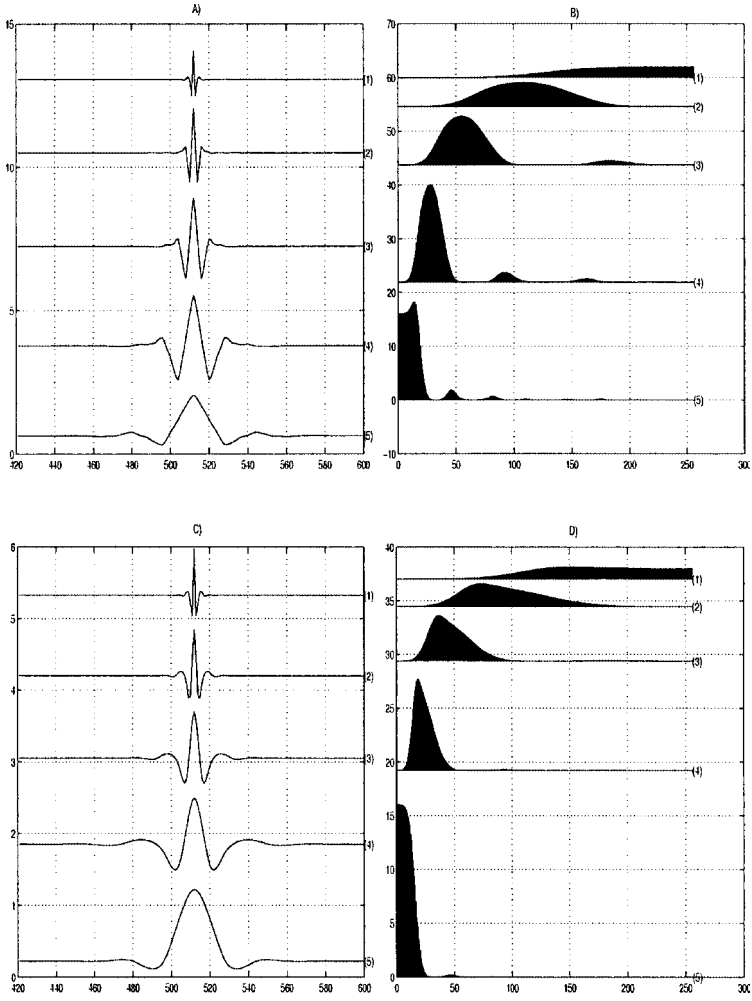


FIG. 7. (A) The decomposition wavelets of order 3 $\tilde{\psi}_\beta^l$, $l = 1, \dots, 4$ (lines 1–4) and $\tilde{\varphi}_\beta^l$, $l = 4$ (line 5). (B) Their spectra. (C) The reconstruction wavelets of order 3 ψ_β^l , $l = 1, \dots, 4$ (lines 1–4) and φ_β^l , $l = 4$ (line 5). (D) Their spectra; $\beta^{k+1}(r) = U_3^k(r)/2$, $k = j + 1 - l$.

obtained through the primal filters, ones of the second scale through the dual scheme, and so on. For the wavelets in C, conversely, we started from the dual scheme. All the wavelets are of the thirteenth order and the control filters are $\beta^{k+1}(r) = U_{13}^k(r)/2$, $k = j + 1 - l$, $l = 1, \dots, 4$.

7. DISCUSSION

We presented a construction in lifting mode of a new family of biorthogonal wavelet and wavelet packet transforms and a library of biorthogonal periodic symmetric waveforms. The construction is based on the superconvergence property of interpolatory splines of even degrees, which are used as a predicting aggregate in the lifting scheme. The lifting

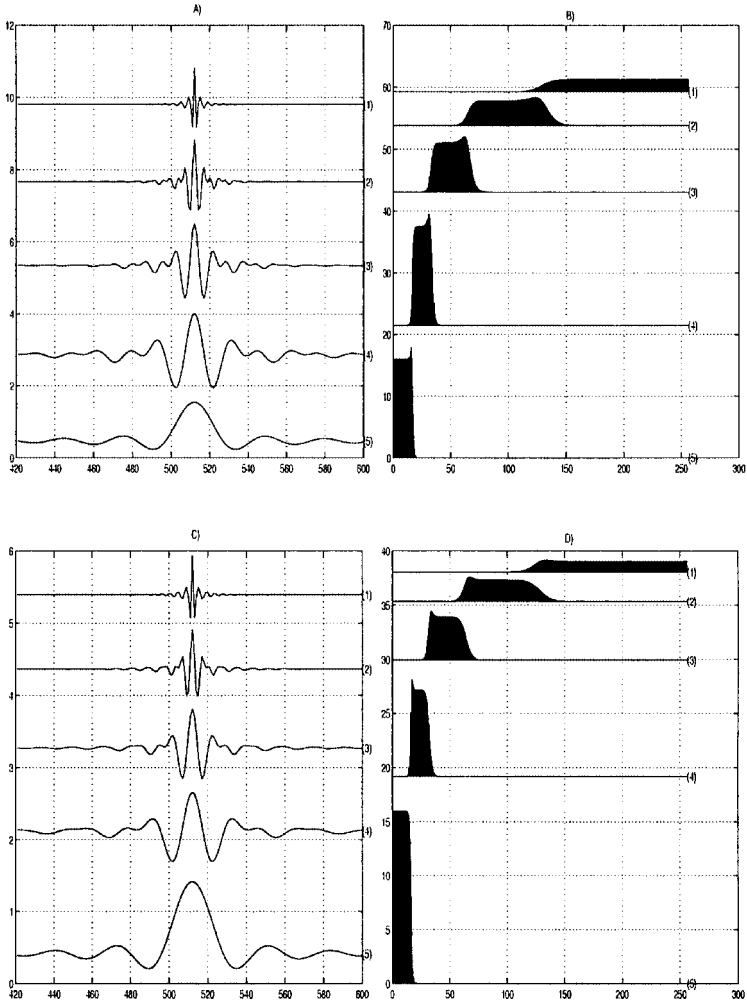


FIG. 8. (A) The decomposition wavelets of order 13 $\tilde{\psi}_\beta^l$, $l = 1, \dots, 4$ (lines 1–4) and $\tilde{\varphi}_\beta^l$, $l = 4$ (line 5). (B) Their spectra. (C) The reconstruction wavelets of order 3 ψ_β^l , $l = 1, \dots, 4$ (lines 1–4) and φ^l , $l = 4$ (line 5). (D) Their spectra. Here $\beta^{k+1}(r) = U_{11}^k(r)/2$, $k = j + 1 - l$.

construction allows more efficient implementation and provides tools for custom design of the filters and wavelets. As is common in lifting schemes, the computations can be carried out “in place” and the inverse transform is performed in a reverse order. The difference with the conventional lifting scheme [20] is that all the transforms are implemented in the frequency domain with the use of the fast Fourier transform FFT. However, to recover the coefficients of the decomposition of a certain level, the inverse FFT is used.

The presented construction of the wavelet packet transforms can be used in adaptive schemes such as matching pursuit [14] and best basis algorithm [8] methodologies. Search for the best basis can be implemented in the frequency domain (without switching into the time domain) provided that the cost function is l_2 norm. The matching pursuit can also be efficiently performed in the frequency domain. The dictionary will be constructed by using a mixture of wavelet packets of different orders.

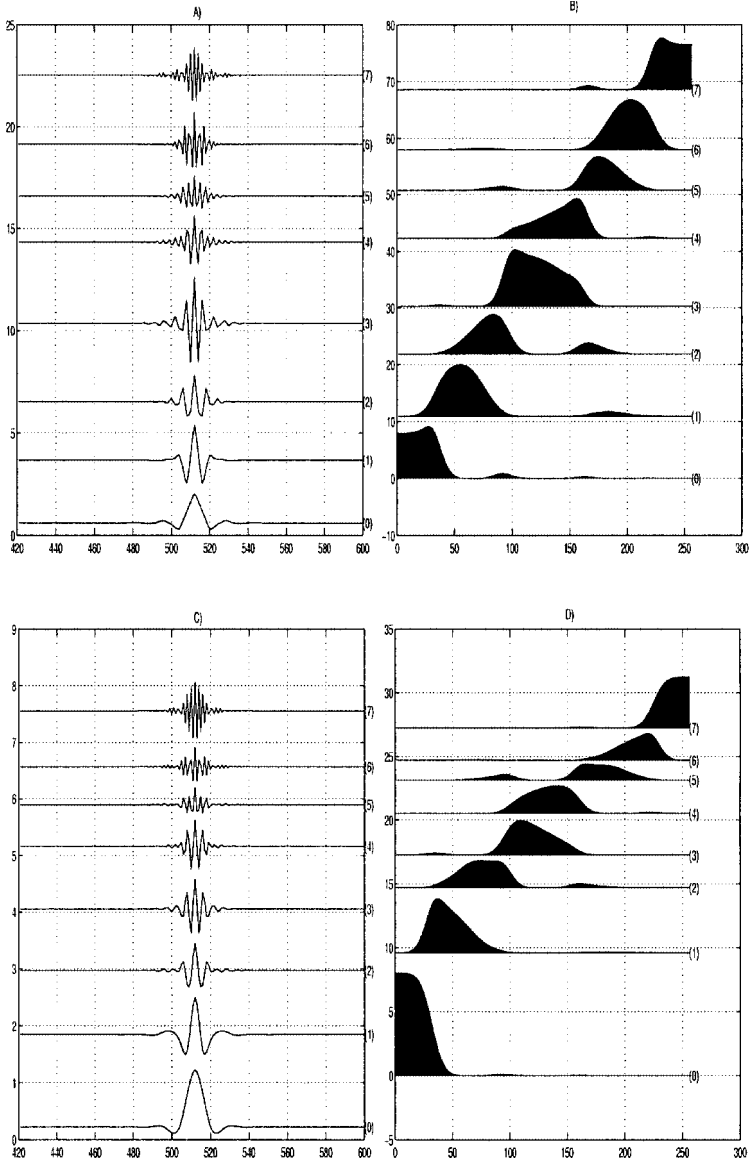


FIG. 9. (A) The decomposition wavelet packets of order 3 of the third scale $\tilde{\psi}_{\beta}^{3,r}$, $r = 0, \dots, 7$. (B) Their spectra. (C) The reconstruction wavelet packets of order 3 of the third scale $\psi_{\beta}^{3,r}$, $r = 0, \dots, 7$. (D) Their spectra. Here $\beta^{k+1}(r) = U_{\beta}^k(r)/2$, $k = j + 1 - l$, $l = 1, 2, 3$.

We used the control tools, which are inherent in the transforms, in order to have the properties of the decomposition filters and waveforms as similar as possible to the properties of the reconstruction filters.

A high-pass decomposition filter in our construction comprises a finite difference block of an order $p + 1$. In a nonperiodic setting, it corresponds to the vanishing moments property up to order p of the corresponding wavelets. Thus, such a filter turns fragments of the signal which (almost) coincide with polynomial of degree p close to zero. The related low-pass filter, on the contrary, leaves the fragments almost intact.

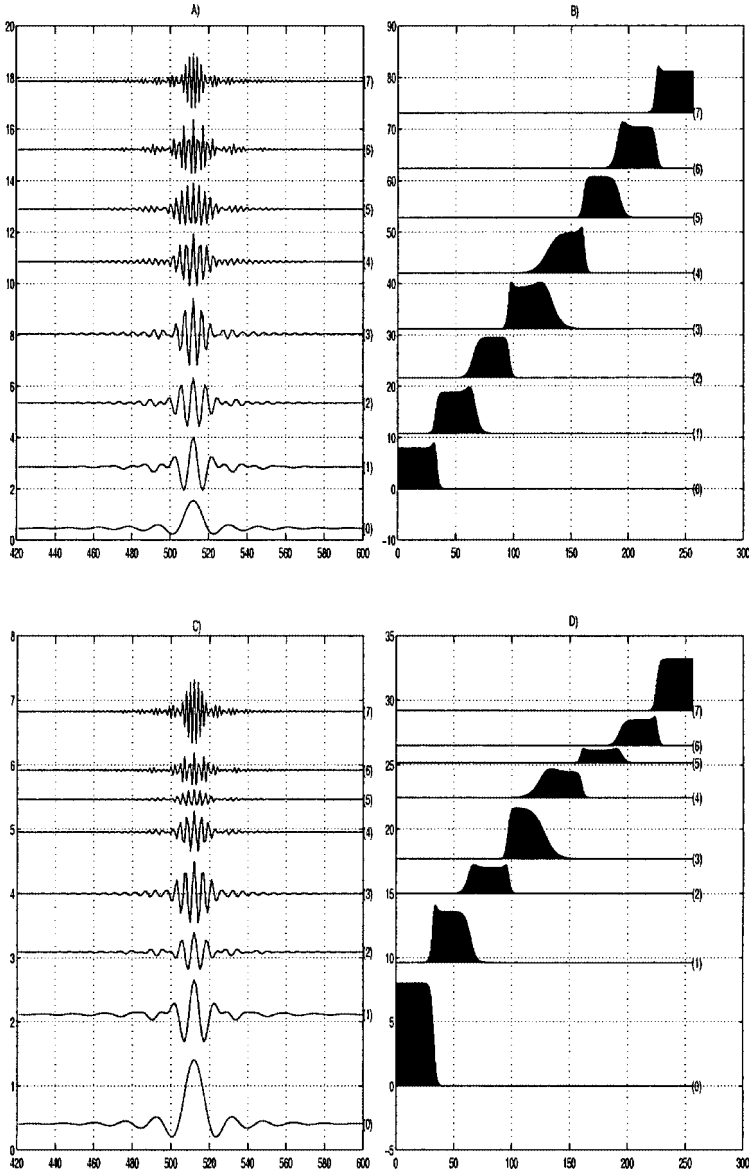


FIG. 10. (A) The decomposition wavelet packets of order 13 of the third scale $\tilde{\psi}_\beta^{3,r}$, $r = 0, \dots, 7$. (B) Their spectra. (C) The reconstruction wavelet packets of order 13 of the third scale $\psi_\beta^{3,r}$, $r = 0, \dots, 7$. (D) Their spectra. Here $\beta^{k+1}(r) = U_{13}^k(r)/2$, $k = j + 1 - l$, $l = 1, 2, 3$.

Our algorithm allows a stable construction of filters comprising differences of very high orders. For examples, we presented the filters associated with differences up to fourteenth order and the recurrence formulas for constructing filters of even higher orders.

The computational complexity of the application of the wavelet transform on a signal of length N is the same as the application of the FFT on the signal, which is $O(N \log_2 N)$. At first glance, it seems to be more computationally expensive than the complexity of the regular wavelet transform, which is $O(N)$. However, we must take into account that

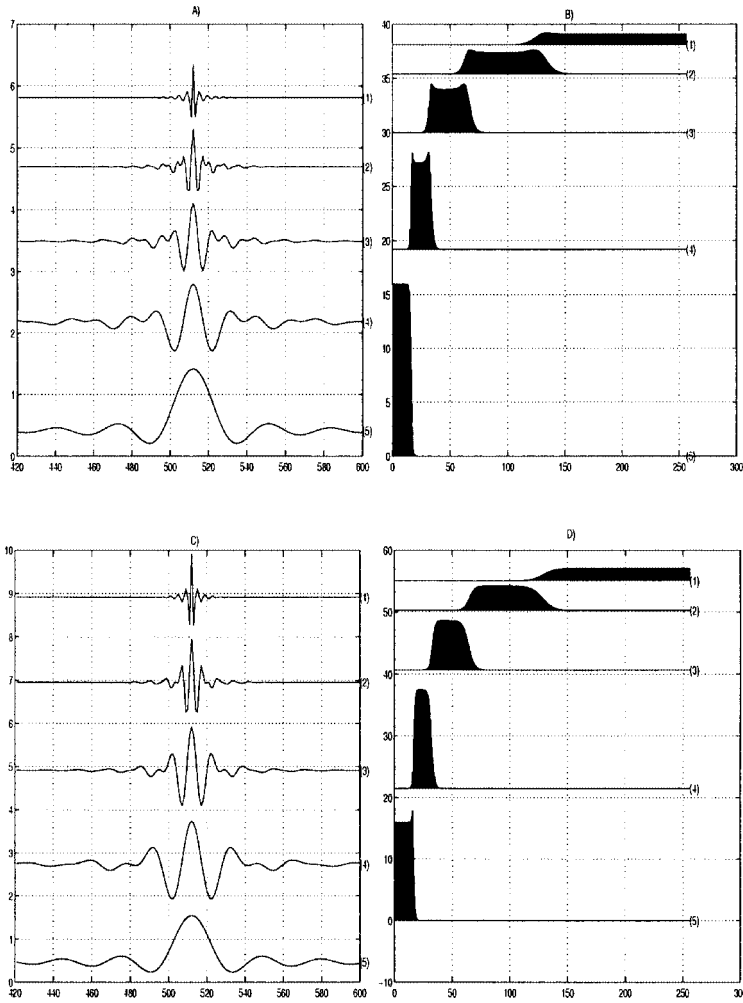


FIG. 11. (A) The wavelets of order 13 constructed by the alternating scheme: first decomposition step is primal. (B) Their spectra. (C) The similar wavelets with first dual step. (D) Their spectra. Here $\beta^{k+1}(r) = U_{13}^k(r)/2$, $k = j + 1 - l$, $l = 1, \dots, 4$.

the complexity of the latter depends linearly on the length of the filters involved which, in turn, increases when the number of vanishing moments increases. For example, the Daubechies filter with 10 vanishing moments is of length 20. On the other hand, increase of the difference order in our scheme does not affect the cost of the implementation. Therefore, especially for higher orders p , the complexity of our algorithm is comparable to if not less than, the complexity of the standard wavelet transform. However, we hope to reduce the complexity of the algorithms more in time- rather than in frequency-domain implementation. To achieve this, we plan to abandon the periodic setting. Such an implementation must use recursive filters. To accelerate the performance, we intend to employ the factorization technique developed in [4]. This will be the subject of our next paper. By now it is done in [3] for a similar scheme which employed discrete rather than continuous interpolatory splines.

We should particularly emphasize that our scheme is based on interpolation and, as such, it involves only samples of signals and it does not require any use of quadrature formulas. This property is valuable for signal and image processing.

Also of great importance to these applications is the fact that these filters have linear phase property and the basic waveforms are symmetric. In addition, these filters yield perfect frequency resolution.

We anticipate a wide range of applications for the presented library of waveforms in signal and image processing, especially for problems where refined resolution of the frequency domain is required. Recently, we successfully applied the devised wavelet packets in an algorithm for acoustic recognition [2].

REFERENCES

1. A. Aldroubi, M. Eden, and M. Unser, Discrete spline filters for multiresolutions and wavelets of l_2 , *SIAM Math. Anal.* **25** (1994), 1412–1432.
2. A. Z. Averbuch, E. Hulata, V. A. Zheludev, and I. Kozlov, A wavelet packet algorithm for classification and detection of moving vehicles, *Multidimensional Syst. Signal Process.* **12** (2000), 1053–1086.
3. A. Z. Averbuch, A. B. Pevnyi, and V. A. Zheludev, Butterworth wavelets derived from discrete interpolatory splines: Recursive implementation, *Signal Process.* **81** (2001), 2363–2382.
4. A. Z. Averbuch, F. G. Meyer, and J.-O. Strömberg, Fast adaptive wavelet packet image compression, *IEEE Trans. Image Process.* **9** (2000), 792–800.
5. G. Battle, A block spin construction of ondelettes. Part I. Lemarié functions, *Comm. Math. Phys.* **110** (1987), 601–615.
6. C. K. Chui and J. Z. Wang, On compactly supported spline wavelets and a duality principle, *Trans. Amer. Math. Soc.* **330** (1992), 903–915.
7. A. Cohen, I. Daubechies, and J.-C. Feauveau, Biorthogonal bases of compactly supported wavelets, *Comm. Pure Appl. Math.* **45** (1992), 485–560.
8. R. R. Coifman and M. V. Wickerhauser, Entropy-based algorithms for best basis selection, *IEEE Trans. Inform. Theory* **38** (1992), 713–719.
9. W. Dahmen, B. Han, R.-Q. Jia, and A. Kunoth, Biorthogonal multiwavelets on the interval: Cubic Hermite splines, IGPM-Preprint 147, January 1998, revised February 1999; to appear in *Constr. Approx.*
10. G. Deslauriers and S. Dubuc, Interpolationion dyadique, in “Fractals, Dimensions nonentières et applications,” Masson, Paris, 1987.
11. G. Deslauriers and S. Dubuc, Symmetric iterative interpolation processes, *Constr. Approx.* **5**, (1989), 49–68.
12. D. L. Donoho, Interpolating wavelet transform, Preprint 408, Department of Statistics, Stanford University, 1992.
13. P. G. Lemarié, Ondelettes à localization exponentielle, *J. Math. Pures Appl.* **67** (1988), 227–236.
14. S. Mallat and Z. Zhang, Matching pursuit with time-frequency dictionaries, *IEEE Trans. Signal Process.* **41** (1993), 3397–3415.
15. I. J. Schoenberg, “Cardinal Spline Interpolation,” CBMS, Vol. 12, SIAM, Philadelphia, 1973.
16. I. J. Schoenberg, Contribution to the problem of approximation of equidistant data by analytic functions, *Quart. Appl. Math.* **4** (1946), 45–99, 112–141.
17. G. Strang and T. Nguen, “Wavelets and Filter Banks,” Wellesley-Cambridge Press, Cambridge, MA, 1996.
18. J. O. Strömberg, A modified Franklin system and higher order spline systems on \mathbb{R}^n as unconditional bases for Hardy spaces, in “Proceedings of Conference in Honor of Antoni Zygmund” (W. Becker, A. P. Calderón, R. Fefferman, and P. W. Jones, Eds.), Vol. II, pp. 475–493, Wadsworth, New York, 1981.
19. Yu. N. Subbotin, On the relation between finite differences and the corresponding derivatives, *Proc. Steklov Inst. Math.* **78** (1965), 24–42.

20. W. Sweldens, The lifting scheme: A custom design construction of biorthogonal wavelets, *Appl. Comput. Harmon. Anal.* **3** (1996), 186–200.
21. M. Unser, A. Aldroubi, and M. Eden, A family of polynomial spline wavelet transforms, *Signal Process.* **30** (1993), 141–162.
22. M. Vetterli and C. Herley, Wavelets and filter banks: Theory and design, *IEEE Trans. Signal Process.* **40** (1992), 2207–2232.
23. W. V. Wickerhauser, “Adapted Wavelet Analysis from Theory to Software,” AK Peters, Wellesley, MA, 1994.
24. V. A. Zheludev, Periodic splines and the fast Fourier transform, *Comput. Maths Math. Phys.* **32** (1992), 149–165.
25. V. A. Zheludev, Spline harmonic analysis and wavelet bases, Proc. Symp. Appl. Math., Vol. 48, pp. 415–419, Amer. Math. Soc., Providence, RI, 1994.
26. V. A. Zheludev, Periodic splines, harmonic analysis, and wavelets, in “Signal and Image Representation in Combined Spaces,” Wavelet Anal. Appl. (Y. Y. Zeevi and R. Coifman, Eds.), Vol. 7 pp. 477–509, Academic Press, San Diego, CA, 1998.